OF-WTWI-1984-33

POROSITY DISTRIBUTION TRENDS IN WOLFCAMP STRATA OF THE PALO DURO BASIN, TEXAS PANHANDLE - IMPLICATIONS FOR GROUND-WATER FLOW THROUGH PERMIAN DEEP-BASIN AQUIFER

R. D. Conti
P. Wirojanagud

CAUTION

This report describes research carried out by staff members of the Bureau of Economic Geology that addresses the feasibility of the Palo Duro Basin for isolation of high-level nuclear wastes. The report describes the progress and current status of research and tentative conclusions reached. Interpretations and conclusions are based on available data and state-of-the-art concepts, and hence, may be modified by more information and further application of the involved sciences.

Prepared for the
U.S. Department of Energy
Office of Nuclear Waste Isolation
under contract no. DE-AC-97-83WM46615

Bureau of Economic Geology
W.L. Fisher, Director
The University of Texas at Austin
University Station, P.O. Box X
Austin, Texas 78713

1984

Porosity Distribution in Wolfcamp Series, Palo Duro Basin, Texas Panhandle--Implications for Ground-Water Flow through Deep-Basin Aquifer

R. D. Conti and P. Wirojanagud

ABSTRACT

Average-porosity distributions in the Wolfcamp deep-basin aquifer are studied to discern the geographic trends in effective porosity throughout the Palo Duro Basin. Highly resolved, log-derived porosity data are used to improve porosity resolution in computer-simulated areal ground-water modeling. Assessing vertical distributions of lithology and porosity in each of the wells studied involves cross-plotted neutron- and density-porosity log responses which more accurately identify lithology and porosity than cross-plotted neutron-porosity and acoustic (interval travel time) responses. Subsequent analyses of log-derived porosity distributions yield information about the total effective-pore volume (movable water) in the Wolfcamp aquifer, in addition to enhancing the accuracy of estimating deep-brine velocities and travel times in its basin-wide traverse. Northeastward, basin-wide travel times range between 2.5×10^5 and 2.0×10^6 years, indicating differential frequency of basin flushing across the basin.

INTRODUCTION

Overview of Wolfcamp Stratigraphy

The transition of the Palo Duro Basin from a relatively deep basin to a shallow restricted carbonate platform is recorded within the Wolfcamp sedimentary record. Precambrian uplifts, subaerially exposed at the end of the

Pennsylvanian, were completely covered by shallow-marine deposits by the end of Wolfcampian time (Dutton and others, 1982). Wolfcamp strata, which consist of carbonate and terrigenous-clastic sedimentary rocks, include sediments deposited in environments ranging from deep-marine to shallow shelf and delta platforms. Basically, the framework facies of the Wolfcamp series were dominated by (1) fan-delta systems, (2) high-constructive delta systems, (3) carbonate shelf and shelf-margin systems and (4) slope and basin systems (Handford, 1980).

According to Handford (1980), Wolfcamp strata were deposited within the following sedimentary scenario. Arkosic-sand and gravel terrigenous clastics, eroded from adjacent highlands, and transported by streams to the margins of the Palo Duro Basin, were deposited in prograding fan-delta systems south of the Amarillo Uplift. Concomitantly, high-constructive deltas were being built in the southeastern part of the basin. Sediments of these deltas are composed mostly of subarkosic sands and muds shed off the Ouachita tectonic belt to the east. Alternating delta-lobe advances and carbonate-bank building resulted in shelf-margin progradation in the eastern part of the basin. Because deltaic sedimentation was absent in the western part of the basin, western shelf margins did not prograde, but instead were built by vertically aggraded carbonate sediments.

By the end of Wolfcampian deposition, the shelf margins had migrated as far south as the Matador Arch. Wolfcampian sedimentation had transformed a once, relatively deep basin into "an extensive, low-relief back-shelf environment" (Dutton and others, 1982), and tectonic events that initially (pre-Wolfcamp) dominated localized-basin development had shifted to a larger scale of influence, manifest by "regional subsidence which resulted in burial of the uplifts" (Goldstein, 1984). Later Early Permian (Wichita) sedimentation was dominated by evaporite deposition in extensive sabkha plains and landward by

continental sedimentation as evidenced by Wichita anhydrites and red beds overlying the Brown Dolomite. "Because Wolfcamp strata were deposited during a marine regression, the top of the Wolfcampian Series is actually a time-transgressive boundary that is older in the northern part of the basin than in the south" (Dutton and others, 1982).

Wolfcamp Correlations

The base of the Wolfcamp, which is equivalent to the top of the Pennsylvanian, has been mapped by Dutton (Dutton and others, 1982). Parameters used to define this Pennsylvanian-Permian boundary include (1) lithostratigraphic sample-log correlations and (2) paleontological (fusulinid) data (Dutton and others, 1982).

The Brown Dolomite is the oldest post-Pennsylvanian carbonate unit that is correlatable across the entire basin. For purposes of this paper, it is treated as a stratigraphic group (fig. 1) although it is generally considered an informal stratigraphic unit. Its "top is generally picked at the boundary between a porous, coarsely crystalline buff dolomite, and the (relatively nonporous) overlying anhydritic dolomite of the Wichita group" (Dutton and others, 1982). The base of the Brown Dolomite is likewise defined by the deepest extent of the Wolfcamp strata's uppermost porous dolomite.

Porosity-Distribution Studies in Geological Waste-Isolation Studies

The Wolfcamp Series (fig. 1) which Bassett and Bentley (1983) describe as a deep-basin brine aquifer within the Palo Duro Basin (fig. 2) lies beneath bedded San Andres salt, a potential host for isolating high-level nuclear waste. Because of its stratigraphic proximity below the Permian salt, the Wolfcamp is a possible hydrologic conduit for transporting radionuclides if

they were to leak from overlying salt beds. According to Davis (1980) failed containment of deeply buried radioactive waste would probably result in radionuclides being transported by ground water. Predicting the future of ground-water motion is therefore imperative, and an understanding of effective porosity distributions within the Wolfcamp (deep-basin) aquifer is significant because the interconnected pore spaces are the permeable pathways that formation water flows through. Understanding the distribution of porous zones is essential for evaluating the amount of movable water contained in the Wolfcamp, and ultimately for estimating travel times of deep brine and frequency of basin flushing.

A study of porosity distributions in the Wolfcamp strata was initiated for the purpose of recognizing effective-porosity distribution relative to depositional environments and ultimately its influence on the Palo Duro Basin's ground-water dynamics. Previous Wolfcamp subsurface-stratigraphy studies have relied almost entirely on correlations of resistivity and self-potential curves, gamma logs and sample logs (Handford, 1980; Handford and others, 1981). Such studies yielded only generalized indications of porosity and lithology distributions.

In this study, log-derived porosity has been recognized by simultaneous interpretation of neutron, density, gamma and caliper logs. The contribution of fracturing to porosity enhancement has not been considered because interpretation of the above suite of logs does not distinguish between pore space introduced through fracturing and other types of porosity. The effects of fracturing are therefore not included in this paper's results.

Porosity--General Remarks

Porosity, Ø, is a dimensionless parameter that is expressed as a percentage or fraction. It is the volume of void spaces in a rock, V_v, divided

by the total unit volume of the rock, V_t, so that

$$\phi = \frac{V_v}{V_t}$$

Because Wolfcamp strata are mostly carbonate rocks, discussion of porosity focuses on pore systems as they apply to limestone and dolomite. Carbonate porosity, which is created and modified by numerous processes, is erratic and unpredictable as compared to that of sandstones, and is generally not very great (Wilson, 1975). It can form when organisms secrete skeletal carbonate, creating chambers or other void spaces, or when sediments compact gravitationally, shrink by desiccation, fracture by tectonic forces or dissolve by chemical reactions. Porosity can form by organisms boring or burrowing. Many stages of development, destruction or modification may occur during the rock's diagenesis so that "the many possible processes of porosity creation and modification, operating through a long depositional and diagenetic history, make genetic as well as physical complexity the norm in sedimentary carbonates" (Choquette and Pray, 1970).

Porosity Discernment in Potential Waste-Isolation Environments

Porosity values are obtained from a variety of individual geophysical logs, either directly or through calculations (when lithology is known), but for the best resolution of porosity data, plotting one log response against another is generally most useful (Keys and Brown, 1973).

Cross plotting one porosity-log response against another is frequently done to identify lithology and make accurate porosity estimates (Burke and others, 1969). Because neutron, density and sonic logs reflect lithology, porosity and fluid content, porosity values can be calculated in rocks of known monomineral lithology when only one porosity log is available. In the Palo

Duro Basin, however, Wolfcamp strata are often lithologically complex, unpredictable in extent and equivocally correlatable. Each porosity log registers responses to the rock's unique physical properties, so that simultaneous analysis of two logs allows for an interpretation by which the logs' separate responses to different minerals yield quantitative differences in mineralogy and porosity (Borneman and Doveton, 1983; Fertl, 1981).

Sample logs, which are records of lithology with depth, usually provide only qualitative porosity information, derived from cuttings, for the intervals where visual porosity is observed. Whereas sample logs often reflect interpretive variances and possible contamination from cavings (Borneman and Doveton, 1983) porosity logs offer direct recordings of physical responses with depth. The obvious advantage of making porosity determinations through cross-plotting porosity-log reponses is that a record of quantitative porosity values with depth can be made with much greater accuracy than that resulting from sample-log analysis.

METHODOLOGY

Comparison of Neutron-Density and Neutron-Sonic Cross-Plotting Methods for Identifying Lithology and Porosity

Two basic methods for making quantitative lithology and porosity determinations are prescribed by Schlumberger (1972). Both methods employ plotting one type of porosity-log response against a different porosity-log response. In one method, responses from an acoustic (interval travel time) log are plotted against depth-equivalent responses from a neutron-porosity log. The appropriate Schlumberger chart (1979) is then used to quantitatively evaluate porosity and lithology. In the other method, density-porosity log responses are plotted against neutron-porosity log responses, yielding similar quantitative

determinations of lithology and porosity. Examining both methods for their relative accuracy, as described below, indicates that the neutron-density method is superior to the neutron-sonic method for identifying lithology and porosity in Wolfcamp strata.

Lithologic logs of Wolfcamp core (Bureau of Economic Geology, unpublished at vertical scale: 1 inch = 10 ft) from U.S. Department of Energy (DOE) test holes document control intervals of 100 percent limestone and 100 percent dolomite against which cross-plot-derived lithologies are compared. Laboratory analyses of core plugs provide porosity control, against which cross-plot-derived porosities are compared.

Pure-carbonate Wolfcamp core was recovered from U.S. Department of Energy (DOE test holes in Donley County, Stone and Webster Engineering Corporation Sawyer No. 1 (3082-3924 ft; 939-1196 m), Oldham County; Stone and Webster Engineering Corporation, Mansfield No. 1 (4502-4990 ft; 1372-1520 m); and Swisher County, Stone and Webster Engineering Corporation, Zeeck No. 1 (5472-5618 ft; 1668-1712 m). After depths of pure-carbonate intervals were recorded at 2- to 10-foot (0.61-3.05 m) increments (depending on the extent of vertical continuity of the pure limestone and dolomite) correlatable neutron-porosity and density-porosity values were read from Schlumberger's Simultaneous Compensated Neutron-Formation Density Log (Schlumberger trademark) (for the Stone and Webster Engineering Corporation Sawyer No. 1 and Mansfield No. 1 wells) and from the Simultaneous Compensated Neutron-Litho Density Log (Schlumberger trademark) (for the Stone and Webster Engineering Corporation Zeeck No. 1 well) and then recorded. Interval-transit-time values were read from Schlumberger's Borehole Compensated Sonic-Log (Schlumberger trademark) for all three DOE test holes and recorded.

After depth-equivalent neutron-porosity, density-porosity, and interval-transit-time values were all recorded, they were plotted onto Schlumberger

chart CP-1d (Schlumberger, 1979) for neutron-density cross-plotting analysis (figs. 3 and 4) and Schlumberger chart CP-2b (Schlumberger, 1979) for neutron-sonic cross-plotting analysis (figs. 5 and 6).

A comparison of the neutron-density cross-plotting method (fig. 3) with the neutron-sonic method (fig. 5) for pure-dolomite intervals reveals that the data cluster more closely to the dolomite line in neutron-density plotting (fig. 3) than they do in neutron-sonic plotting (fig. 5), indicating the neutron-density method yields more accurate identification of dolomite. Neutron-density plotting (fig. 3) also shows higher maximum-porosity values than those in neutron-sonic plotting (fig. 5). In neutron-density plotting (fig. 3) the maximum porosity identified in the Stone and Webster Engineering Corporation Sawyer No. 1 well equals 27%. In neutron-sonic plotting (fig. 5) the maximum dolomite porosity in the same well equals 21%. Neutron-density maximum dolomite porosity in the Stone and Webster Engineering Corporation Mansfield No. 1 and Zeeck No. 1 wells equals 21% (fig. 3). Neutron-sonic maximum dolomite porosity in the same wells, respectively, equals 19% and 17% (fig. 5). Lower maximum porosity and inferior lithologic identification resulting from neutron-sonic cross plotting (fig. 5) are probably due to the sonic log's inability to detect secondary porosity (Burke and others, 1969; Schlumberger, 1972; Fertl, 1981; MacCary, 1983).

A comparison of the neutron-density (fig. 4) and neutron-sonic (fig. 6) cross-plotting methods for pure limestone indicates that the limestone data cluster more closely to the limestone line in the former method than in the latter. Again, this indicates a more accurate discernment of carbonate lithology through neutron-density cross plotting. As in the above dolomite example, neutron-density plotting consistently yields higher maximum porosities than the neutron-sonic method. Maximum porosity identified by neutron-density plotting

in Stone and Webster Engineering Corporation Sawyer No. 1 pure limestone (fig. 4) equals 30%. The maximum limestone-porosity identified by neutron-sonic plotting in the same well (fig. 6) equals 25%. Maximum limestone porosities identified by neutron-density plotting in Stone and Webster Engineering Corporation Mansfield No. 1 and Zeeck No. 1 wells equal 28% and 22%, respectively (fig. 4), whereas the maximum limestone porosities identified by neutron-sonic plotting in the same wells, respectively, equal 19% and 17% (fig. 6). Again, the lower maximum porosities indicated by the neutron-sonic method are probably due to the sonic log's inability to detect secondary porosity (Burke and others, 1969; Schlumberger, 1972; Fertl, 1981; MacCary, 1983).

Comparison of lithologic determinations derived from the two prescribed cross-plotting methods in (Wolfcamp) pure dolomite and pure limestone reveals greater variation in lithologic identity is consistently found by employing the neutron-sonic cross-plotting method. This is especially true for the pure limestone intervals studied. Neutron-sonic responses in pure-limestone intervals (fig. 6) yield identifications of silica, anhydrite and salt, in addition to greatly differing ratios of limestone/dolomite. The pure-limestone neutron-density responses (fig. 4), however, indicate only limestone/dolomite and limestone/silica lithology ratios. Silica identified by neutron-density plotting (fig. 4) almost always coincides with chalcedony replacement of fossil fragments, or chert contamination, as indicated in core logs.

Determining Vertical and Lateral (Geographic) Distributions of Porosity and Lithology

To understand the vertical and lateral distributions of porosity and lithology, twenty-seven neutron-density logs (Table 1) of Wolfcamp strata were analyzed, using Schlumberger's (1979) neutron-density cross-plotting charts. Each log's density-porosity and neutron-porosity values, resolved from two to

ten feet were recorded by depth. Log-header data regarding type of neutron-log response (i.e., sidewall-neutron porosity or compensated-neutron porosity) and drilling-fluid density dictates which Schlumberger (1979) Log Interpretation Chart is applicable.

Plotting neutron-porosity against density-porosity responses yields relative percents of dolomite, limestone and silica (i.e., sandstone, granite wash or chert), the presence of anhydrite (where overlying the Brown Dolomite), and porosity. Porosity is shown to be effective in all lithologies identifiable by cross plotting (Senger and others, 1984). Shales, although not directly identified by cross plotting, are characterized by intervals with anomalously high neutron and density porosities, greater than 30%, enlarged borehole (indicated by caliper response), and relatively high gamma values of greater than 100 API units. Intervals with porosities greater than 25%, enlarged borehole and gamma values less than 100 API units were interpreted as sandy shale. Although the shale and sandy-shale intervals are characterized by anomalously high porosity values, presumably due to the presence of flocculated clay minerals, their effective porosities are interpreted to equal 0%.

Empirical justification exists for claiming effective-porosity determinations can be made from cross-plotted neutron- and density-log responses. Generally, porosity determinations made by laboratory analyses of core plugs correlate well ($r = 0.68$) with the porosity values determined from cross plotting neutron-porosity against density-porosity responses. If probable footage slips that can occur during core recovery are accounted for, $r = 0.93$. Additionally, data generated from laboratory analyses of core plugs suggest that permeability increases with increasing porosity in a log-normal relation (Senger and others, 1984).

Cross-plot-derived parameters include lithologic identifications consisting of anhydrite, dolomite/limestone, limestone/silica and their respective porosities. Lithology and porosity data are assimilated graphically into litho-porosity columns (vertical scale: 1 inch = 50 ft) for each of the twenty-seven wells studied, but are not included in this paper.

Weighted-Average-Porosity Calculations

Weighted-average porosity was determined for each well for the Brown Dolomite and for the entire Wolfcamp Series to discern their geographic distributions of effective porosity within the Palo Duro Basin. Weighted averages were calculated by the following general equation using the data in Table 2 for each well, in the stratigraphic intervals described above.

$$\text{Weighted-Average Porosity} = \frac{\sum_{\emptyset = 0\text{-}5\%}^{>30\%} (\text{net thickness of each 5\% } \emptyset \text{ range})(\text{mean } \emptyset \text{ of each 5\% } \emptyset \text{ range})}{\sum_{\emptyset = 0\text{-}5\%}^{>30\%} (\text{net thickness of each 5\% } \emptyset \text{ range})}$$

Derived weighted-average-porosity values are mapped in figures 7 and 8. This study of average-porosity geographic distributions, although lacking the necessary well control to establish detailed porosity distributions and correlations, is a first attempt to quantify Wolfcamp porosity distributions in the Palo Duro Basin, and provides a quantitative means of assessing porosity values and their relation to the depositional environments interpreted by Handford (1980).

Determining Total Effective-Pore Volume

Initial conclusions which show that log-derived porosity in nonshaly lithofacies is equivalent to effective porosity (Senger and others, 1984) make it possible to estimate the total effective-pore volume of the Wolfcamp deep-basin aquifer. In order to understand the relative porosity distributions of the Brown Dolomite and the entire Wolfcampian Series strata, porosity distributions were studied collectively in figures 7 and 8 and separately in figures 9-21. The relatively high porosity that characterizes the Brown Dolomite is readily recognized by its porosity-log signature and typified in litho-porosity columns by predominantly dolomite lithology and high porosity.

The technique used to assess Wolfcamp total-effective pore volume in the Palo Duro Basin is similar to those described by Dahlberg (1979) and Seni and Jackson (1983). From the litho-porosity columns, net thicknesses of seven (integer) porosity ranges (0-5%, >5-10%, >10-15%, >15-20%, >20-25%, >25-30%, and >30%), shown in figures 9-21, were evaluated as shown in Table 2. Net thickness of each porosity range for each well was mapped and contoured so that three-dimensional representations of each porosity-range's net thickness resulted (figs. 9-21). Through planimetry-based calculations, volumes of slices between contour lines are individually estimated, then summed to yield the total volume of sediments hosting each porosity range in the Wolfcampian Series, as summarized in Table 3. The mean-porosity value of each porosity range (i.e., 2.5% for the 0-5% porosity range) were multiplied by the total volumes (of sediments hosting each porosity range) and summed to compute the total effective porosity within the Wolfcamp strata as shown in Table 3. For the >30% porosity range, an assigned mean-porosity value of 32.5% was used to compute pore volume in the very-high-porosity sediments. Total effective pore

volume for the entire Wolfcampian Series equals 2.91×10^{13} ft^3 (8.24×10^{11} m^3).

RESULTS

Average-Porosity Distributions: Wolfcamp Series

Effective porosity within the Lower Permian Wolfcamp strata of the Palo Duro Basin is distributed throughout limestone, nonstratal-dolomite, arkosic-sands and granite-wash sediments. Of these, there are more carbonate rocks than coarse-grain clastic sediments in the Wolfcamp strata. Large volumes of Lower Wolfcamp shales and sandy shales have assumed noneffective porosity.

Vertical distributions of rock type and void-space systems are characterized in litho-porosity columns discussed above. From these columns, net-thickness of each of seven porosity ranges were summed (Table 2) and mapped as shown in figures 9-15.

Weighted-average-porosity values, mapped for each well, yield average-effective-porosity trends in Wolfcamp sediments, as shown in figure 7. Essentially, the highest average porosities are found in the northern part of the basin; lower average porosities are found in the eastern and western parts of the basin; the lowest average porosities are found in the central and southern parts of the basin. Average porosities were not determined for specific lithologies, but rather for the entire stratigraphic interval, between the top of the Brown Dolomite (equivalent to the top of the Wolfcamp) and the top of the Pennsylvanian strata. The highest-average-porosity trend is found in the northern part of the basin, with the axis of highest porosity approximately oriented south-southeast, and passing through Oldham, Deaf Smith, and Castro Counties. The highest-average-porosity trend, in the northern part of the basin, is generally associated with alternating, high-porosity clastic and

carbonate sediments that were probably deposited in shelf-margin and back-shelf environments during their basinward progradation.

The lowest-average-porosities are along the eastern, western and southern shelf margins, and are due mostly to the presence of shales and sandy shales, which have assumed effective-porosity values of 0% and, consequently, greatly reduced average-porosity values. The shales and sandy shales found near or landward of the shelf margins are probably associated with prodelta or inter-deltaic, fine-grained clastic sedimentation.

Average-Porosity Distributions: Brown Dolomite

The Brown Dolomite, generally regarded as the top of the Wolfcamp (Dutton and others, 1982) in the Palo Duro Basin, is characterized by its predominantly dolomite lithology and relatively high porosity. Distinctive lithologic and porous character allow for picking a unique interval in litho-porosity columns, thus facilitating porosity-distribution analyses shown in figures 16-21.

Estimating weighted-average porosities yields average-porosity trends for the Brown Dolomite interval, as shown in figure 8. Generally, the highest average porosities in the Brown Dolomite are found in the southeastern and northern areas of the basin, basinward of the Lower Wolfcampian shelf margin interpreted by Handford (1980). In the southeastern part of the basin, the axis of highest porosity is oriented north-northwest along the Middle Wolfcampian shelf margin, passing through Motley, Floyd, and Briscoe Counties. In the northwestern part of the basin, Brown Dolomite axes of high porosity pass through Swisher and central Deaf Smith and Randall Counties. The lowest average-porosity trend in the Brown Dolomite is found in the southern part of the basin, just north of the Matador Arch, in south-central Hale and southeastern Lamb Counties.

Considering the time-transgressive nature of the Brown Dolomite (Dutton and others, 1982), the above trends indicate that the uppermost unit of the Wolfcamp strata developed progressively lower-porosity systems in younger basinward and southward prograded carbonates.

Porosity-Range Distributions: Wolfcamp Series

In general, as shown by figures 9 and 10, low-porosity sediments in the Wolfcamp strata are thickest along the central-basin axis, which is oriented north-south through eastern Hale and central Swisher Counties, and north-northwest through eastern Randall County. This suggests the basin axis' function as a depocenter for shales and fine-grain clastic sediments, which ultimately develop little effective porosity. The basin axis described here differs from the axis mapped by Budnik and Smith (1982) in that south of the Randall/Swisher County boundary, it is oriented north-south. By comparison, Budnik and Smith's axis, which is determined by interpreting isopachus trends, is oriented south-southeast south of the Randall/Swisher County boundary, and passes through Swisher, Briscoe, Floyd, and Motley Counties. The axis of thickest >5-10% porosity (fig. 10), passing through Motley and Briscoe Counties in the southeastern part of the basin is oriented similarly as the Lower Wolfcampian eastern shelf margin.

The axis of greatest thickness for medium-porosity sediments (figs. 11 and 12) is oriented north-south, passing through eastern Oldham and Deaf Smith Counties, where it is basinward of the Lower Wolfcampian western shelf margin. In the eastern part of the basin, most axes of greatest thickness are oriented northwest-southeast, parallel to and just basinward of the Lower Wolfcampian eastern shelf margin. In the southeastern part of the basin, the axes of greatest thickness coincide with the high-constructive delta systems described by Handford (1980).

Generally, axes of greatest thickness for high-porosity sediments (figs. 13, 14, and 15) are related to locally significant geologic features such as prograding delta systems. Most high-porosity sediments are of clastic origin, and were shed off of subaerially exposed, structurally positive basement rocks during early-to-middle Wolfcampian deposition. In southeastern Oldham County high-porosity arkosic sediments were shed off the Precambrian granite of the Bravo Dome (Nicholson's, 1960, "Oldham Nose" in fig.1). In Randall, Armstrong and Donley Counties, the high-porosity sediments coincide with arkosic sands being shed off the Precambrian highlands of the Amarillo Uplift in the northeastern part of the basin. Just north of the Matador Arch, in the southeastern area of the basin, high-porosity sediments coincide well with Handford's (1980) high-constructive delta systems.

The highest-porosity sediments, those with >30% porosity (fig. 15), are thickest in Deaf Smith and Oldham Counties, in the northwestern part of the basin, where most of the high-porosity intervals consist of several individual beds of sand, less than 5 ft thick, in the basal Wolfcamp strata. Of notable exception is a limestone interval with predominantly oomoldic porosity observed in core from the Oldham County Mansfield No. 1 well (4820-4830 ft) and detected in porosity-log analysis and verified by core examination. This particular interval shows abnormally low permeability for its correspondingly high porosity in core-plug analysis, indicating the noneffectiveness, or lack of interconnectedness between oomoldic pore spaces.

Porosity-Range Distributions: Brown Dolomite

Generally, axes of thickness for the low-, medium-, and high-porosity ranges are not so closely related to shelf margin systems interpreted by Handford (1980) as are the axes of greatest thickness for the entire Wolfcampian Series strata.

Low-porosity Brown Dolomite (figs. 16 and 17) is of greatest thickness in the eastern part of the basin. The axis of greatest thickness for 0-5% porosity Brown Dolomite (fig. 16) is landward of and parallel to the Lower Wolfcampian eastern shelf margin. The axis of greatest thickeness for >5-10% porosity Brown Dolomite is oriented north-south, passing through central Floyd and Briscoe, and eastern Armstrong Counties, oblique to the northwest-oriented Lower Wolfcampian eastern shelf margin.

Medium-porosity Brown Dolomite (figs. 18 and 19) are not well-defined relative to Wolfcampian shelf margins, but generally the thickest occurrence is in the southeastern part of the basin in Floyd, Motley and Hall Counties. In the north-central part of the basin, three axes of maximum thickness radiate from central Randall County. Clockwise, the three axes are oriented north-northwest, east-southeast, and southwest, as shown in figures 18 and 19. The north-northwest axis is basinward and parallel to the Lower Wolfcampian eastern shelf margin. The east-southeast axis is subparallel to and intersects the Lower Wolfcampian eastern shelf margin. The southwest axis is subnormal to the Lower and Middle Wolfcampian western shelf margins. An axis of overthickened, medium-porosity Brown Dolomite is also found in eastern Hall County, where it is oriented north-south. This easternmost occurrence of medium-porosity dolomite overlies the Hale Positive (Birsa, 1977), is landward of Handford's (1980) Lower Wolfcampian eastern shelf margin, and consequently may have resulted from early, supratidal dolomitization associated with a structural high.

High-porosity Brown Dolomite (figs. 20 and 21) is found in three separate locations in Oldham, Deaf Smith and Randall Counties, where they all occur basinward of Handford's (1980) Lower Wolfcampian shelf margins, in the northern part of the basin. In the eastern part of the basin (eastern Hall County), a net thickness of 5 feet is reached for high-porosity Brown Dolomite, and is

probably associated with the southern limit of the Hall Positive discussed by Birsa (1977).

The proximity of Brown Dolomite (with >20% porosity) to the Lower Wolfcampian shelf margins is an enigmatic feature. Because consensus (Dutton and others, 1982; Handford, 1980) indicates Brown Dolomite is the youngest Wolfcampian stratigraphic unit (informal) and axes of porosity development coincide with the Lower Wolfcampian shale margins, which are some of the oldest basinal features, the following initial conclusions are reached: (1) the Wolfcampian shelf margins were more temporally and geographically stable than Handford (1980) suggests, so as to influence porosity development and dolomitization along shelf margins or (2) the Lower Wolfcampian shelf-margin systems influenced post-depositional hydrologic phenomena to the extent that dolomitization of shelf-margin carbonates was most extensive proximal to paleoshelf margins.

APPLICATION OF POROSITY DATA

Hydrologic Implications of Using Average-Effective-Porosity Distributions in Areal Ground-Water Flow Simulation

Because of its relation to ground-water flow velocity, effective porosity is an important parameter in studying ground-water flow. A better knowledge of the effective-porosity distribution therefore improves the accuracy of flow-rate and travel-time estimates. "The present hydrologic setting was put into motion by the tilting of (the Palo Duro Basin's stratigraphic) units to the east during the Laramide orogeny. Higher elevations west of the Palo Duro Basin in the Sacramento and Sierra Grande Uplifts provide recharge to the flow systems. Lower elevations east of the Palo Duro Basin in the Hardeman Basin, where deep-basin ground-water potentials rise to near land surface, provide potential discharge from the flow systems" (Smith, in preparation).

This section of the report illustrates the comparative results of using some typical-porosity values versus distribution of log-derived porosity (for Wolfcamp Series) in a two-dimensional areal flow model of the Wolfcamp aquifer. Detailed description of the numerical model is available in a report by Wirojanagud and others (1984).

The result of using typical-porosity values, 8% for carbonates, 14% for granite wash, and 5% for shale, is shown in figure 22. Almost all flow in the Wolfcamp aquifer is northeastward. The travel time between two marks on each of the flow lines represents 100,000 years, so that the smaller the distance between two marks, the smaller the velocity. Employing the typical-porosity values for the different lithologies yields a variety of basin-wide traverse times for the deep-aquifer waters. The southeasternmost flow lines indicate that the basin-wide traverse time for water equals about 3.8 million years. In the central part of the basin, a northeastward traverse of deep brines in the Wolfcamp takes about 2.0 million years. In the northwestern part of the basin, basin-wide traverses range between 0.25 and 0.5 million years. Such large differences in basin-wide traverse times result from potentiometric surface (i.e., flow direction) considerations and the geometry of the basin.

As discussed above, average porosity values for Wolfcamp Series sediments were determined for each of the wells studied. Plotting and contouring the data yields a map showing the geographic distribution of average Wolfcamp porosity (fig. 7). This log-derived data base, used in the areal ground-water flow model, resulted in figure 23. All ground-water flow parameters, except porosity, are the same in both simulations. Therefore, simulation results, in terms of head distribution and stream lines, are the same. Only resulting flow velocities, and, hence, basin-wide travel times differ.

The main difference between the two simulation results is that the fluid velocities, derived from incorporating log-derived average porosities, are greater than the velocities derived from using typical porosity values. In the log-derived-porosity model (fig. 23) the southeasternmost flow line indicates that the basin-wide traverse time for water equals about 2.1 million years. In the centrally located flow lines, a northeastward traverse of fluid through the basin takes about 1.0 million years. In the northwesternmost area of the basin deep-brine basin-wide traverses occur on the order of about once every 0.25 to 0.5 million years. Generally, basin-wide travel times are less in figure 23 than they are in figure 22, implying greater fluid velocities in the model that incorporates log-derived average-porosity data. This initial conclusion about travel time and fluid velocity is essentially valid for the entire basin.

Total effective-pore volume, calculated for the Wolfcamp aquifer, equals the quantity of water flushed through the deep-basin porous strata in a given amount of time. The flush rates derived from the typical-porosity flow model (fig. 22) can be compared with the flush rates estimated from using the log-derived-porosity model (fig. 23). The average frequency of basin flushing equals once every 2.0 million years and 1.2 million years, from figures 22 and 23, respectively.

Porosity-Distribution Surveys: Implications for Waste-Isolation Studies

The implications of porosity-distribution studies for waste-isolation programs include (1) defining potential favorable fairways for hydrocarbon-resource exploration and (2) resolving deep-brine velocities in order to estimate transport times for radionuclides which would have potential for leaking into the deep-brine aquifers from a repository in the overlying San Andres bedded salt.

Potentially favorable fairways for hydrocarbon exploration can be identified by evaluating net-thickness trends in medium- and high-porosity sediments. Combined with lithology-distribution, source-rock maturation and structural considerations, porosity quantifications can be used to designate drilling targets in and around preferred sites for high-level nuclear-waste isolation in the Texas Panhandle.

Generally, the axes of highest average porosity for Wolfcampian Series and Brown Dolomite strata coincide with the northern parts of the Lower Wolfcampian shelf margins interpreted by Handford (1980) as shown in figures 7 and 8. The greatest net thickness of medium- and high-porosity carbonate and clastic sediments are also geographically correlatable with northern reaches of Handford's (1980) Lower Wolfcampian shelf margins, as shown in figures 11-15 for Wolfcampian Series strata.

Although the high-average-porosity trends coincide with the shelf margins for the Brown Dolomite (fig. 8), the net thickness trends of medium- and high-porosity are not so correlatable for the Brown Dolomite as they are for the Wolfcampian Series porous intervals. In figures 18 and 19 the axes of thickening medium-porosity Brown Dolomite are oriented subparallel to the shelf margins, except in Randall and Armstrong Counties, where the axes of greatest thickness coincide with the northern part of the Lower Wolfcampian eastern shelf margin. The high-porosity Brown Dolomite net thicknesses, shown in figures 20 and 21, are all proximal to and basinward of Handford's (1980) Lower Wolfcampian shelf margins. The only high-porosity Brown Dolomite that may not be related to the shelf-margin system is in Hall County. Its possible association with a structurally positive basement feature is discussed above.

Deep-basin travel times for brines traveling through porous Wolfcamp strata are indicated in figures 22 and 23. Velocities can be calculated for brine traverses between the western model boundary and the northern basin

boundary. To date, no conclusions can be made with regard to the length of time required for Wolfcamp brines to travel between preferred sites (for high-level nuclear-waste containment) and the biosphere, because no zones of surface discharge (from the deep basin) have as yet been positively identified.

CONCLUSIONS

Neutron-density cross-plotting methods are superior to neutron-sonic methods for making quantitative carbonate-lithology and porosity determinations in the Wolfcamp deep-basin aquifer. The former method was used to discern average-porosity distributions within the predominantly carbonate Wolfcamp Series. Average-porosity data, all calculated from (high-vertical-resolution) lithology/porosity columns were plotted and contoured. The resulting mapped trends compared favorably with those generated through analyses of denser-well-controlled, more qualitative data (see Dutton and others, 1982). This is especially apparent in comparing proximity, linearity and parallelness of the different porosity-range trends with the shelf margins and basin axis. Such trends indicate (1) the Wolfcampian shelf margins were more temporally and geographically stable than Handford (1980) suggests, so as to influence porosity development and dolomitization along shelf margins or (2) the Lower Wolfcampian shelf-margin systems influenced postdepositional hydrologic phenomena to the extent that dolomitization of shelf-margin carbonates was most extensive proximal to paleoshelf margins.

Generally, the map of average-porosity distribution within Wolfcamp strata indicates that the highest average porosities are in the northern part of the basin. Lower average porosities are found in the eastern and western parts of the basin, and the lowest average-porosities are in the southern part of the

basin. The thickest occurrences of high-porosity sediments are related to shelf-margin carbonate and clastic deposition.

The distribution of log-derived average porosity has been incorporated into a ground-water modeling simulation for purposes of refining travel times and velocities of brines flowing through porous Wolfcamp strata. Additionally, quantitative porosity estimates yield information about the total volume of movable water. Estimating the frequency of basin flushing from basin-wide brine traverse times and knowing the total volume of movable water within the Wolfcamp strata allows for approximating the frequency with which one pore volume flows through the deep brine aquifer.

REFERENCES

Adams, J. E., and Rhodes, M. L., 1960, Dolomitization by seepage refluxion: American Association of Petroleum Geologists Bulletin, v. 44, no. 12, p. 1912-1921.

Bassett, R. L., and Bentley, M. E., 1983, Deep-brine aquifers in the Palo Duro Basin: regional flow and geochemical constraints: The University of Texas at Austin, Bureau of Economic Geology Report of Investigations No. 130, 59 p.

Birsa, D. S., 1977, Subsurface geology of the Palo Duro Basin, Texas Panhandle: The University of Texas at Austin, Ph.D. dissertation, 360 p.

Borneman, E., and Doveton, J. H., 1983, Lithofacies mapping in Viola Limestone in south-central Kansas, based on wireline logs: American Association of Petroleum Geologists Bulletin, v. 67, no. 4, p. 609-623.

Budnik, R., and Smith, D., 1982, Regional stratigraphic framework of the Texas Panhandle, in Gustavson, T. C., and others, Geology and geohydrology of the Palo Duro Basin, Texas Panhandle, a report of the progress of nuclear waste isolation feasibility studies (1981): The University of Texas at Austin, Bureau of Economic Geology Geological Circular 82-7, p. 38-86.

Burke, J. A., Schmidt, A. W., and Campbell, R. L., Jr., 1969, The litho-porosity cross plot--a method of determining rock characteristics for computation of log data: The Log Analyst, v. 10, no. 6, p. 25-43.

Choquette, P. W., and Pray, L. C., 1970, Geologic nomenclature and classification of porosity in sedimentary carbonates: American Association of Petroleum Geologists Bulletin, v. 54, no. 2, p. 207-250.

Dahlberg, E. C., 1979, Hydrocarbon reserves estimation from contour maps: a do-it-yourself exercise: Bulletin of Canadian Petroleum Geology, v. 27, no. 1, p. 94-99.

Davis, S. N., 1980, Hydrogeologic effects of natural disruptive events on nuclear-waste repositories (prepared for the Office of Nuclear Waste Isolation under its contract with the U.S. Department of Energy): Pacific Northwest Laboratory, Richland, Washington, 33 p.

Dutton, S. P., Finley, R. J., Galloway, W. E., Gustavson, T. C., Handford, C. R., and Presley, M. W., 1979, Geology and geohydrology of the Palo Duro Basin, Texas Panhandle: The University of Texas at Austin, Bureau of Economic Geology Report of Investigations No. 102, 31 p.

Dutton, S. P., Goldstein, A. G., and Ruppel, S. C., 1982, Petroleum potential of the Palo Duro Basin, Texas Panhandle: The University of Texas at Austin, Bureau of Economic Geology Report of Investigations No. 123, 87 p.

Fertl, W. H., 1981, Openhole crossplot concepts--a powerful technique in well log analysis: Journal of Petroleum Technology, v. 33, no. 3, p. 535-549.

Goldstein, A., 1984, Tectonic controls of Late Paleozoic subsidence in the south-central United States: Journal of Geology, v. 92, p. 217-222.

Handford, C. R., 1980, Lower Permian facies of the Palo Duro Basin, Texas: depositional systems, shelf-margin evolution, paleogeography, and petroleum potential: The University of Texas at Austin, Bureau of Economic Geology Report of Investigations No. 102, 31 p.

Handford, C. R., Dutton, S. P., and Fredericks, P. E., 1981, Regional cross sections of the Texas Panhandle: Precambrian to Mid Permian: The University of Texas at Austin, Bureau of Economic Geology, 8 p. (text) and 7 cross sections.

Keys, W. S., and Brown, R. F., 1973, Role of borehole geophysics in underground waste storage and artificial recharge, in Braunstein, Jules, 1973, Underground waste management and artificial recharge, volume I, sponsored

by American Association of Petroleum Geologists, U.S. Geological Survey and International Association of Hydrological Sciences, p. 147-191.

MacCary, L. M., 1983, Geophysical logging in carbonate aquifers: Ground Water, v. 21, no. 3, p. 334-342.

Nicholson, J. H., 1960, Geology of the Texas Panhandle, in Aspects of the geology of Texas, a symposium: The University of Texas, Austin, Bureau of Economic Geology Publication No. 6017, p. 51-64.

Schlumberger, 1972, Log interpretation, volume I--principles: New York, Schlumberger Limited, 113 p.

Schlumberger, 1979, Log interpretation charts: New York, Schlumberger Limited, 97 p.

Senger, R. K., Smith, D. A., and Conti, R. D., 1984, Preliminary results of porosity and permeability of core plugs, Palo Duro Basin: The University of Texas at Austin, Bureau of Economic Geology Open-File Report OF-WTWI-1984-27.

Seni, S. J., and Jackson, M. P. A., 1983, Evolution of salt structures, East Texas diapir province, part 2: patterns and rates of halokinesis: American Association of Petroleum Geologists Bulletin, v. 67, no. 8, p. 1245-1274.

Smith, D. A., in preparation, Hydraulics of the deep-basin brine aquifer, Palo Duro Basin, Texas Panhandle: The University of Texas at Austin, Bureau of Economic Geology, XX p.

Wilson, J. L., 1975, Carbonate facies in geologic history: Springer-Verlag, 471 p.

Wirojanagud, P., Kreitler, C. W., and Smith, D. A., 1984, Numerical modeling of regional ground-water flow in the deep-brine aquifers of the Palo Duro Basin, Texas Panhandle: The University of Texas at Austin, Bureau of Economic Geology Open-File Report OF-WTWI-1984-8.

FIGURE CAPTIONS

Figure 1. Generalized stratigraphic column and depositional facies, Palo Duro Basin (in Handford, 1980).

Figure 2. Structural elements and general index map of the Texas Panhandle (from Nicholson, 1960, in Dutton and others, 1979).

Figure 3. Neutron-porosity values are plotted against the density-porosity values for "pure" Wolfcamp dolomite. The data cluster more closely to the dolomite line than they do in the neutron-sonic plot for the same intervals (fig. 5). Maximum porosities in the Stone and Webster Engineering Corporation Sawyer No. 1, Mansfield No. 1, and Zeeck No. 1 wells equal 27%, 21%, and 21%. respectively. Generally, the maximum porosities shown in figure 5 are lower for each of the three wells.

Figure 4. Neutron-porosity values are plotted against the density-porosity values for "pure" Wolfcamp limestone. The data cluster more closely to the limestone line than they do in the neutron-sonic plot for the same intervals (fig. 6). Maximum porosities in the Stone and Webster Engineering Corporation Sawyer No. 1, Mansfield No. 1, and Zeeck No. 1 wells equal 30%, 28%, and 22%, respectively. The maximum porosities shown in figure 6 are lower for each of the three wells.

Figure 5. Neutron-porosity values are plotted against the sonic-transit-time values for "pure" Wolfcamp dolomite. The data cluster more closely to the dolomite line in figure 3 than they do in this plot for the same intervals, indicating inferior lithology resolution by neutron-sonic cross plotting. Maximum porosities in the Stone and Webster Engineering Corporation Sawyer No. 1, Mansfield No. 1, and Zeeck No. 1 wells equal 21%, 19%, and 17%, respectively, which are all lower than the maximum porosities shown in figure 3. Lower

maximum porosities are probably due to the sonic log's inability to see secondary and vuggy porosity.

Figure 6. Neutron-porosity values are plotted against the sonic transit time values for "pure" Wolfcamp limestone. The data cluster more closely to the limestone line in figure 4 than they do in this plot for the same intervals, indicating inferior lithology resolution by the neutron-sonic cross plotting method. Maximum porosities in the Stone and Webster Engineering Corporation Sawyer No. 1, Mansfield No. 1 and Zeeck No. 1 wells equal 25%, 19%, and 17%, respectively, which are all lower than the maximum porosities shown in figure 4. Lower porosities are probably due to the sonic log's inability to see secondary and vuggy porosity.

Figure 7. Weighted-average porosity values for the entire Wolfcamp interval.

Figure 8. Weighted-average porosity values for the Brown Dolomite.

Figure 9. Net thickness of the 0-5% porosity range for the Wolfcamp.

Figure 10. Net thickness of the >5-10% porosity range for the Wolfcamp.

Figure 11. Net thickness of the >10-15% porosity range for the Wolfcamp.

Figure 12. Net thickness of the >15-20% porosity range for the Wolfcamp.

Figure 13. Net thickness of the >20-25% porosity range for the Wolfcamp.

Figure 14. Net thickness of the >25-30% porosity range for the Wolfcamp.

Figure 15. Net thickness of >30% porosity range for the Wolfcamp.

Figure 16. Net thickness of the 0-5% porosity range for the Brown Dolomite.

Figure 17. Net thickness of the >5-10% porosity range for the Brown Dolomite.

Figure 18. Net thickness of the >10-15% porosity range for the Brown Dolomite.

Figure 19. Net thickness of the >15-20% porosity range for the Brown Dolomite.

Figure 20. Net thickness of the >20-25% porosity range for the Brown Dolomite.

Figure 21. Net thickness of the >25-30% porosity range for the Brown Dolomite.

Figure 22. Areal model of northeastward ground-water flow in the Wolfcamp deep-basin aquifer, using typical porosity values, as described in the text.

Figure 23. Areal model of northeastward ground-water flow in the Wolfcamp deep-basin aquifer, using average-porosity values derived from plotted and contoured porosity-log analyses, as described in the text and shown in figure 7.

TABLE CAPTIONS

Table 1. List of wells for which neutron-density logs were run to obtain Wolfcamp lithology and porosity determinations.

Table 2. Summary of net thickness of seven porosity ranges in Wolfcamp strata.

Table 3. Summary of volumetric calculations for Wolfcamp strata, based on twenty-seven lithology-porosity columns constructed from neutron-density porosity data.

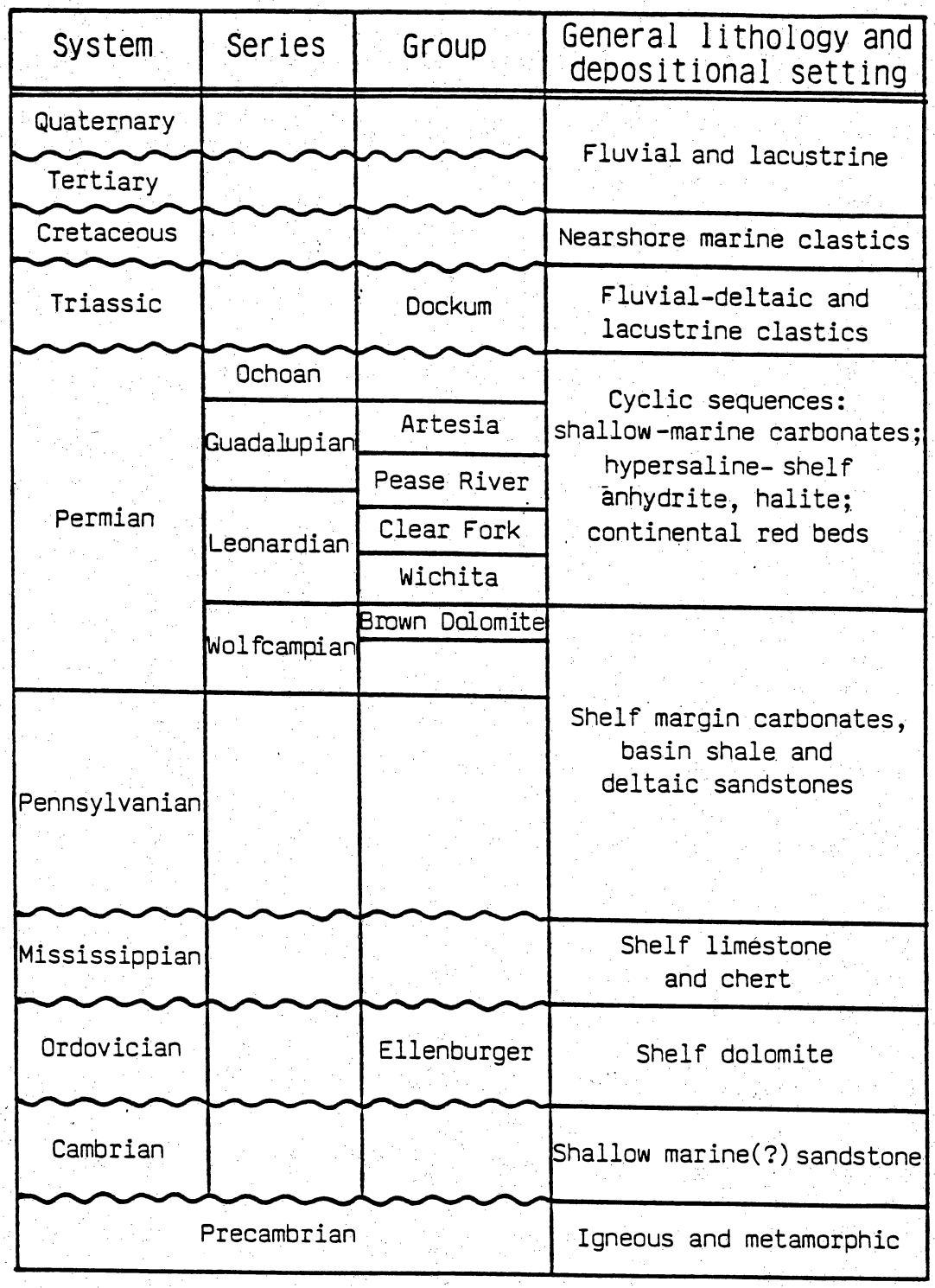

Figure 1. Generalized stratigraphic column and depositional facies, Palo Duro Basin (in Handford, 1980).

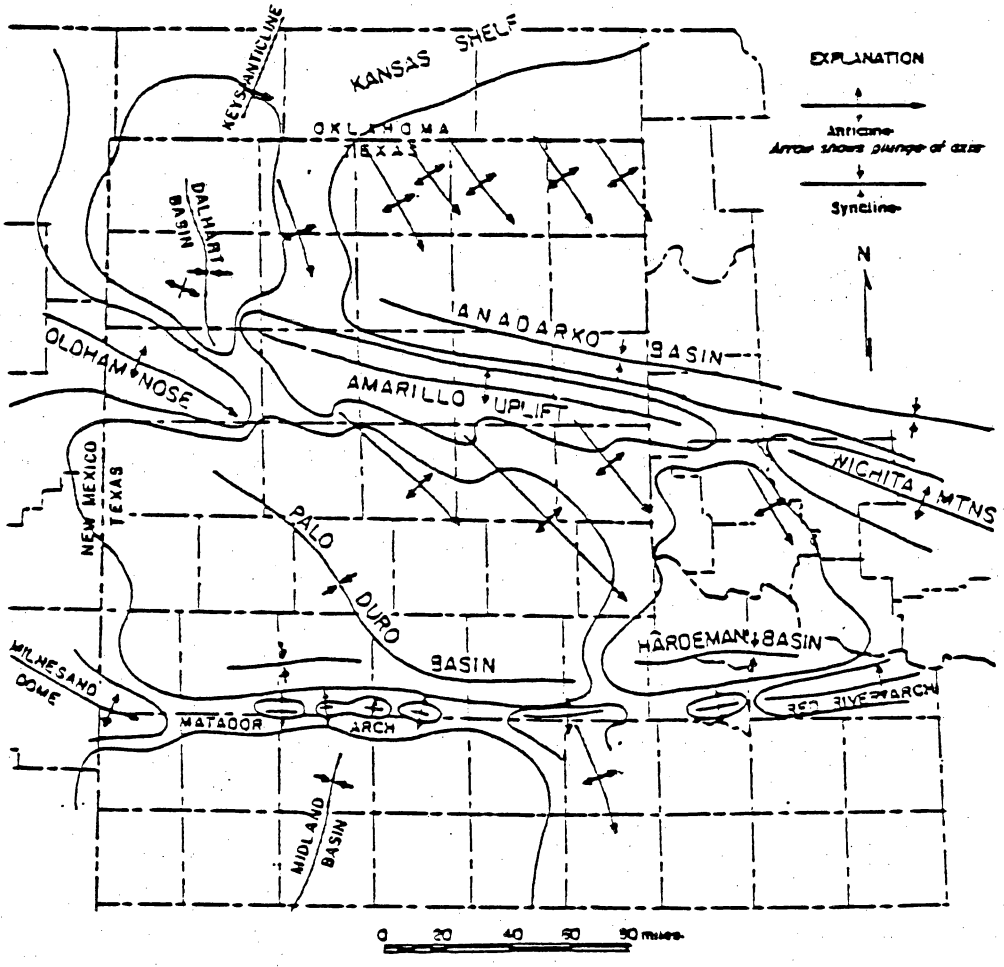

Figure 2. Structural elements and general index map of the Texas Panhandle (from Nicholson, 1960, in Dutton and others, 1979).

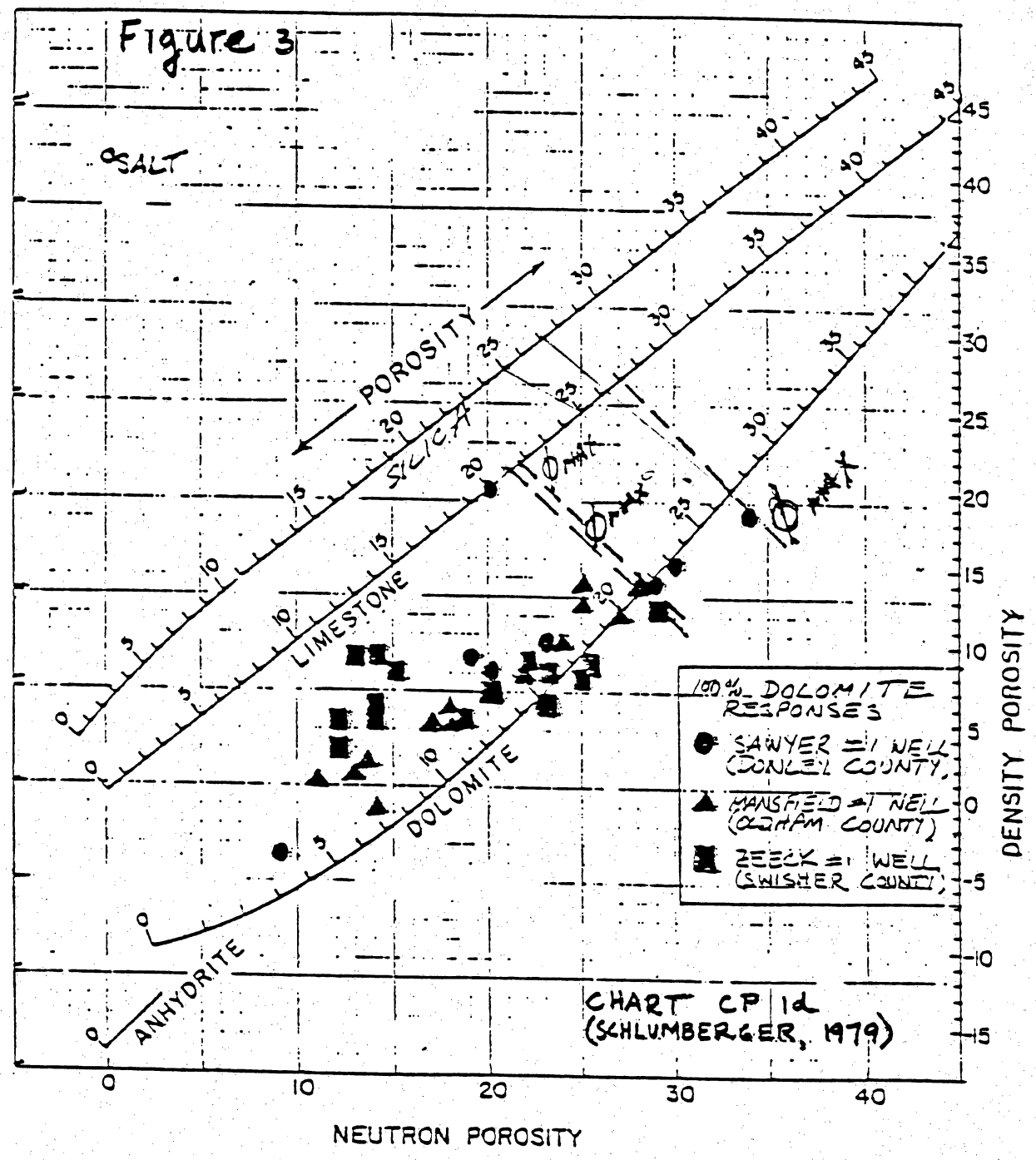

Figure 3. Neutron-porosity values are plotted against the density-porosity values for "pure" Wolfcamp dolomite. The data cluster more closely to the dolomite line than they do in the neutron-sonic plot for the same intervals (fig. 5). Maximum porosities in the Stone and Webster Engineering Corporation Sawyer No. 1, Mansfield No. 1, and Zeeck No. 1 wells equal 27%, 21%, and 21%, respectively. Generally, the maximum porosities show in figure 5 are lower for each of the three wells.

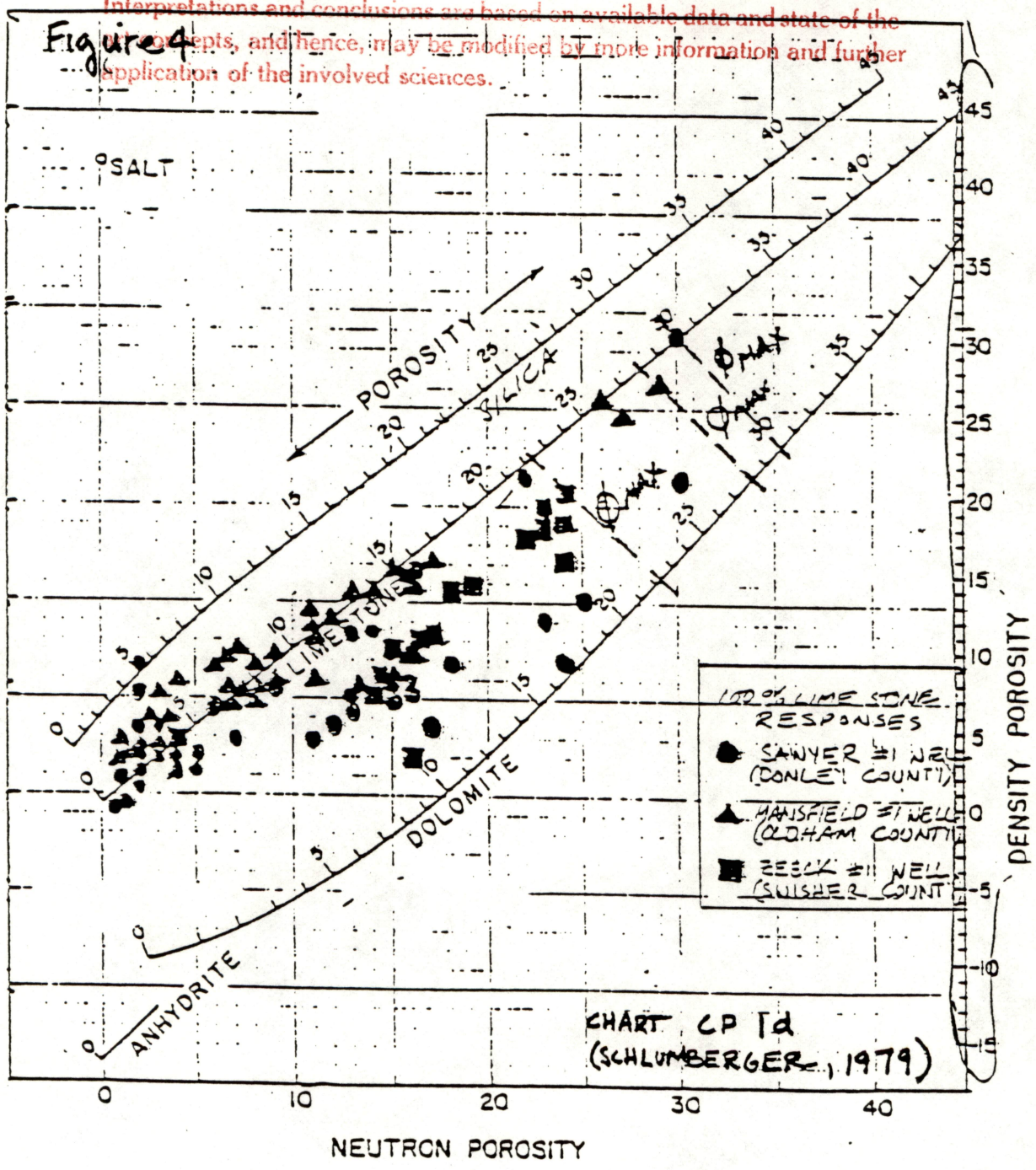

Figure 4. Neutron-porosity values are plotted against the density-porosity values for "pure" Wolfcamp limestone. The data cluster more closely to the limestone line than they do in the neutron-sonic plot for the same intervals (fig. 6). Maximum porosities in the Stone and Webster Engineering Corporation Sawyer No. 1, Mansfield No. 1, and Zeeck No. 1 wells equal 30%, 28%, and 22%, respectively. The maximum porosities shown in figure 6 are lower for each of the three wells.

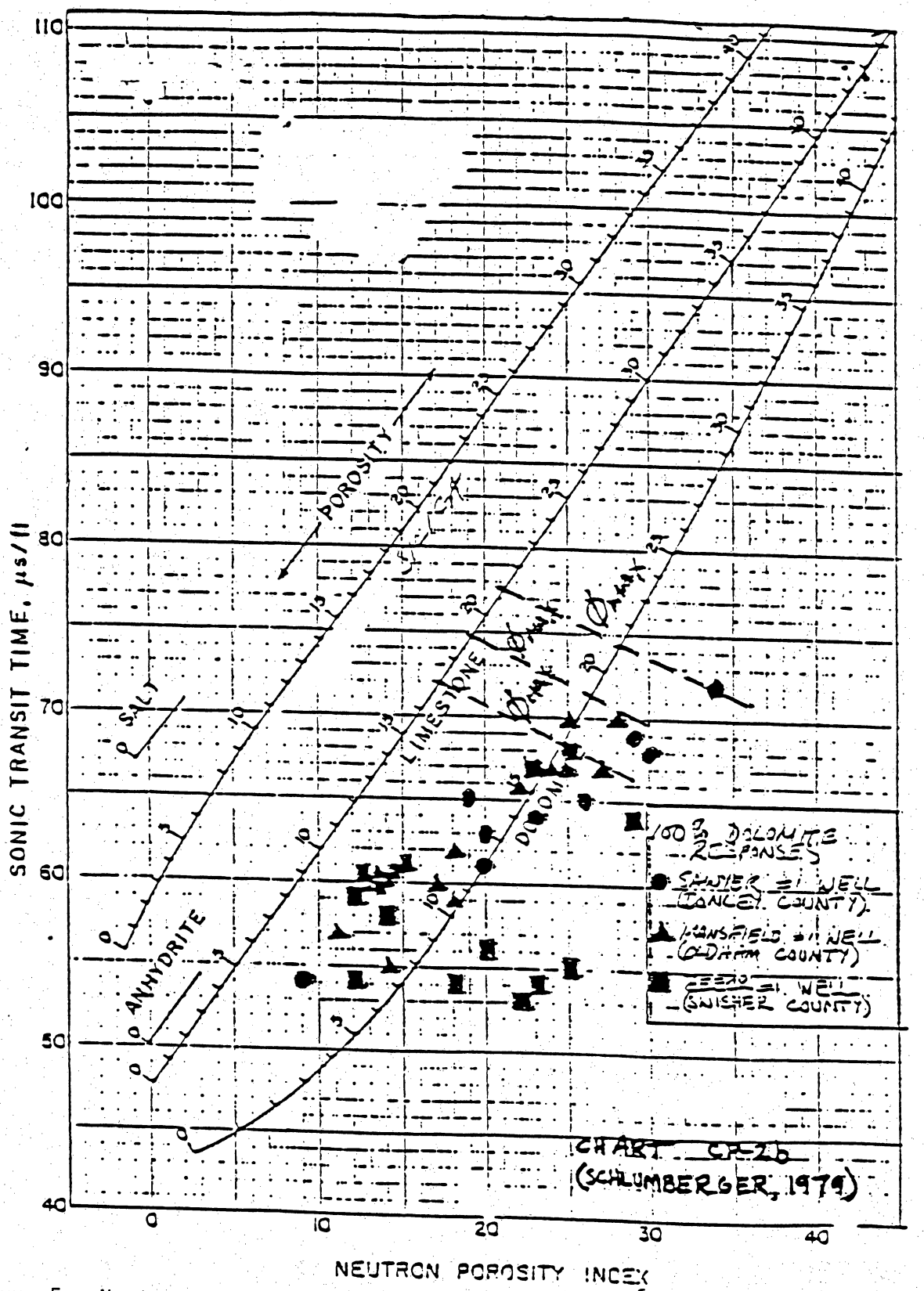

Figure 5. Neutron-porosity values are plotted against the sonic-transit-time values for "pure" Wolfcamp dolomite. The data cluster more closely to the dolomite line in figure 3 than they do in this plot for the same intervals, indicating inferior lithology resolution by neutron-sonic cross plotting. Maximum porosities in the Stone and Webster Engineering Corporation Sawyer No. 1, Mansfield No. 1, Zeeck No. 1 wells equal 21%, 19%, and 17%, respectively, which are all lower than the maximum porosities shown in figure 3. Lower maximum porosities are probably due to the sonic log's inability to see secondary and vuggy porosity.

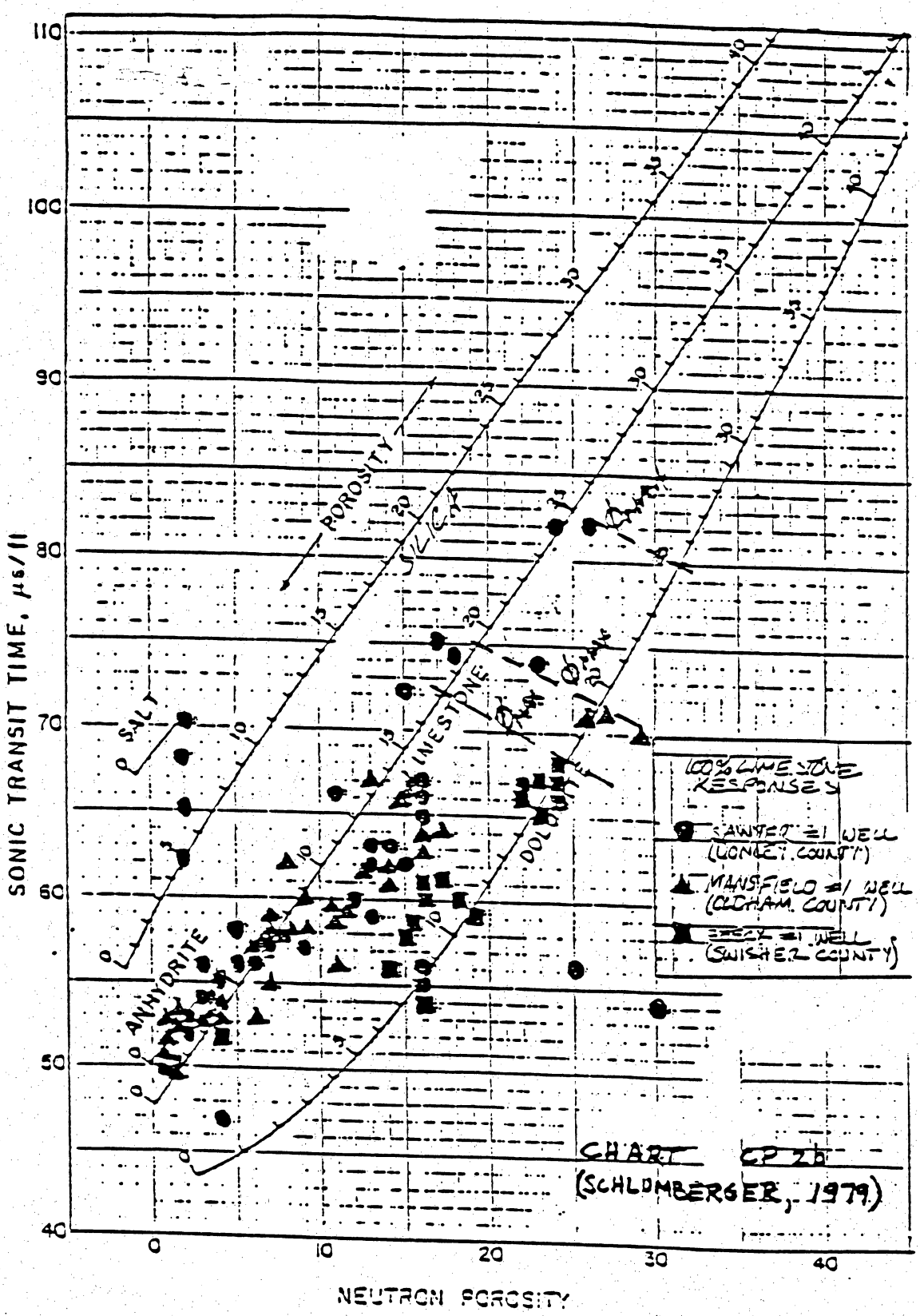

Figure 6. Neutron-porosity values are plotted against the sonic transit time values for "pure" Wolfcamp limestone. The data cluster more closely to the limestone line in figure 4 than they do in this plot for the same intervals, indicating inferior lithology resolution by the neutron-sonic cross plotting method. Maximum porosities in the Stone and Webster Enfineering Corporation Sawyer No. 1, Mansfield No. 1 and Zeeck No. 1 wells equal 25%, 19%, and 17%, respectively, which are all lower than the maximum porosities shown in figure 4. Lower porosities are probably due to the sonic log's inability to see secondary and vuggy porosity.

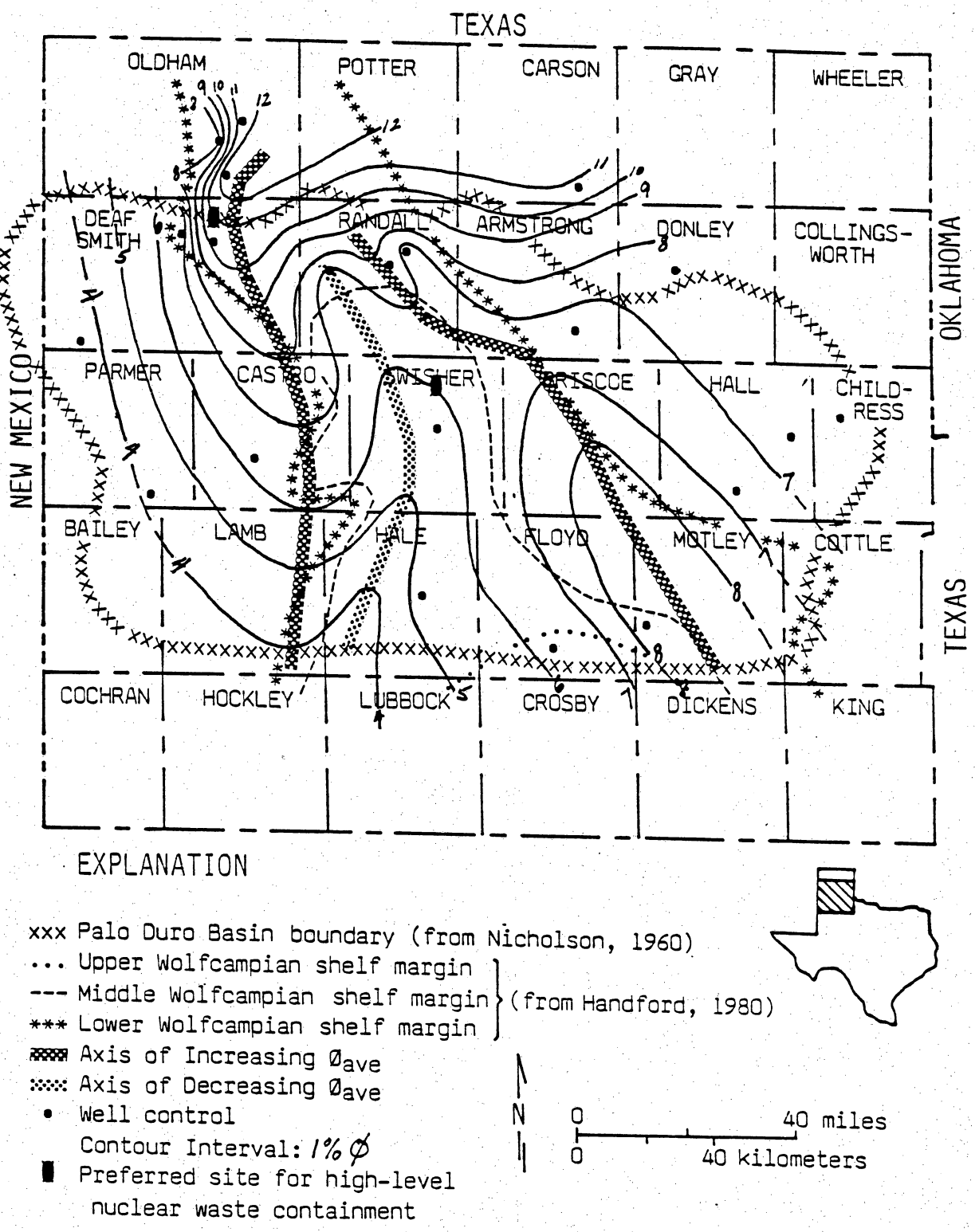

Figure 7. Weighted-average porosity values for the entire Wolfcamp interval.

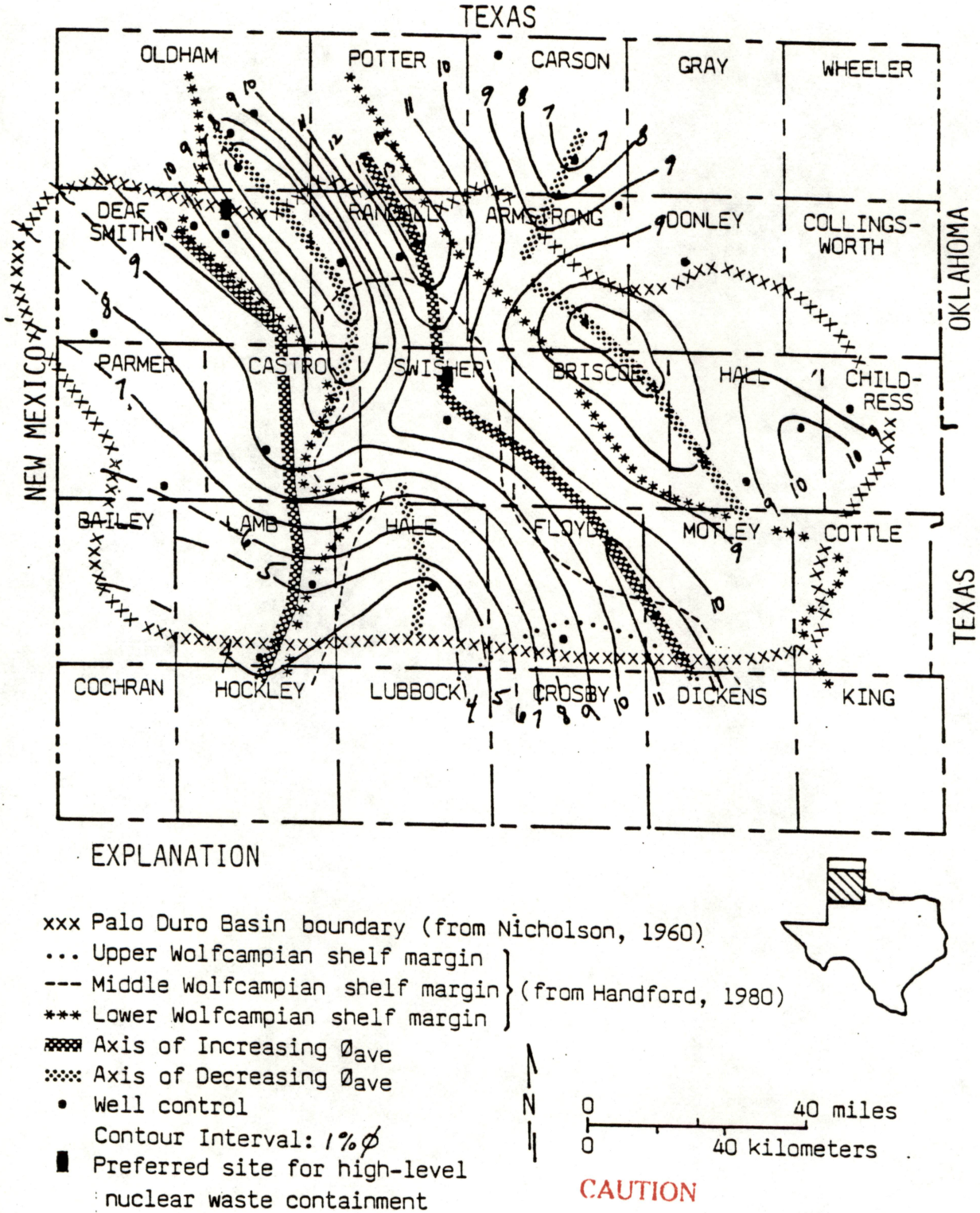

Figure 8. Weighted-average porosity values for the Brown Dolomite.

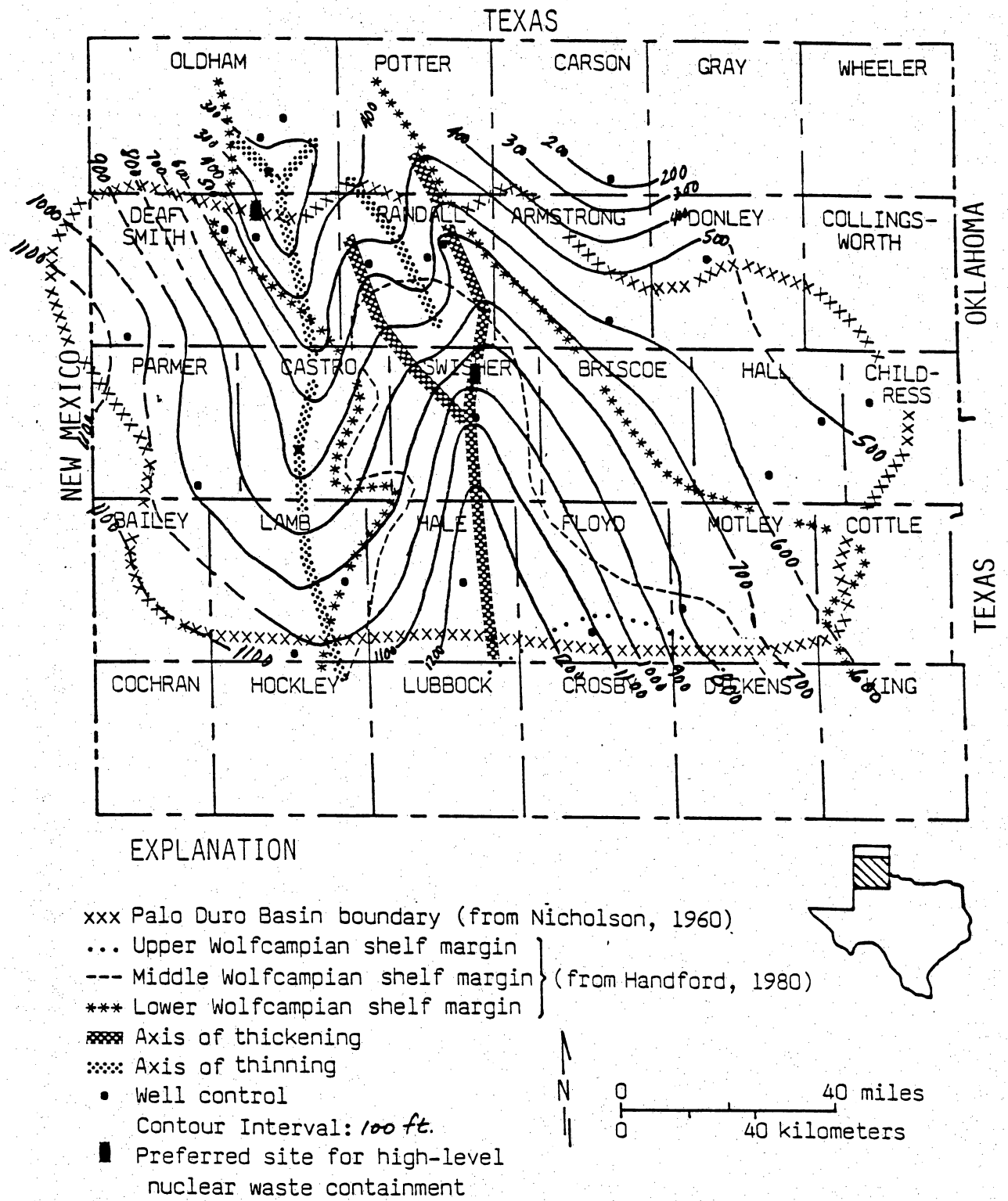

Figure 9. Net thickness of the 0-5% porosity range for the Wolfcamp.

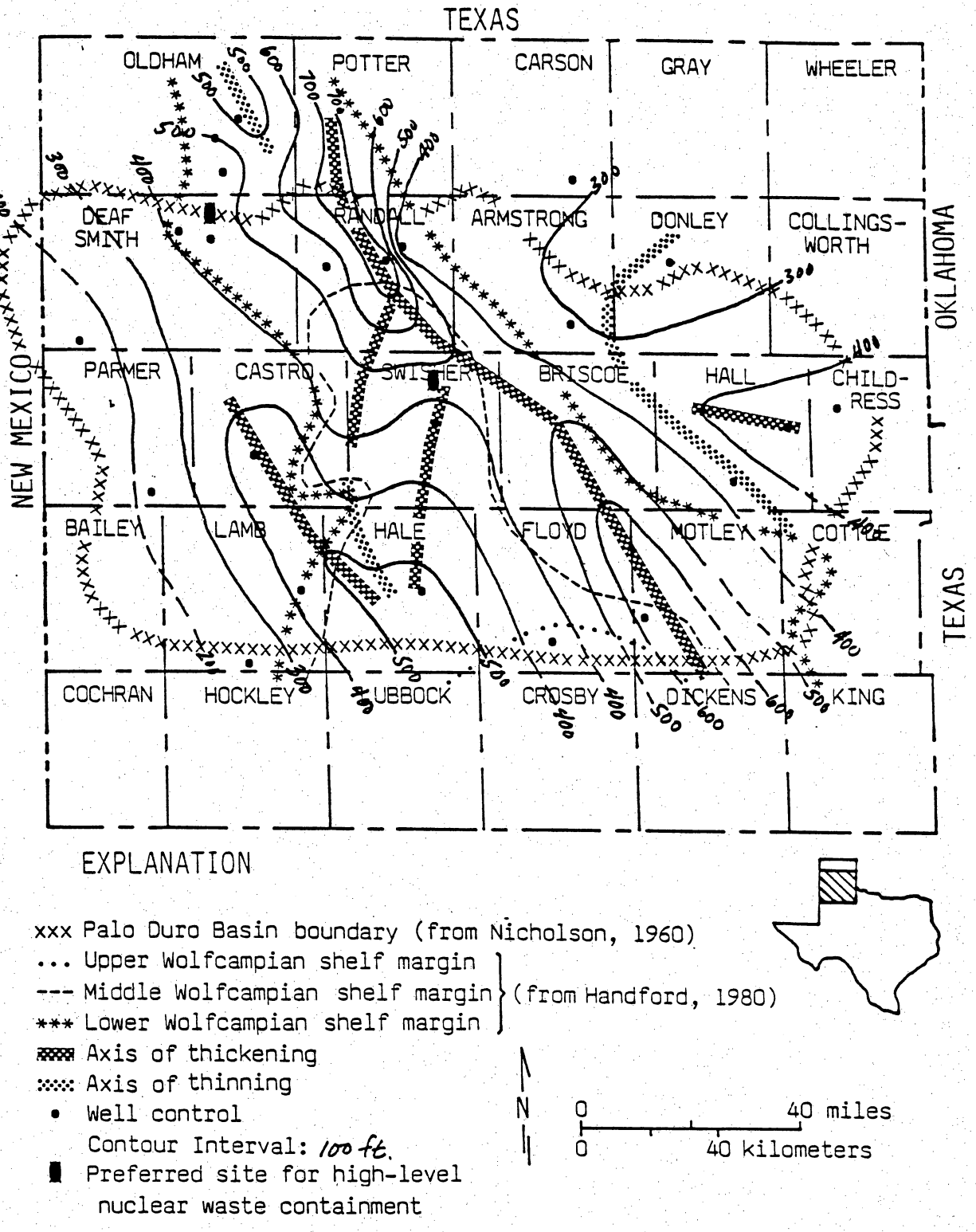

Figure 10. Net thickness of the >5-10% porosity range for the Wolfcamp.

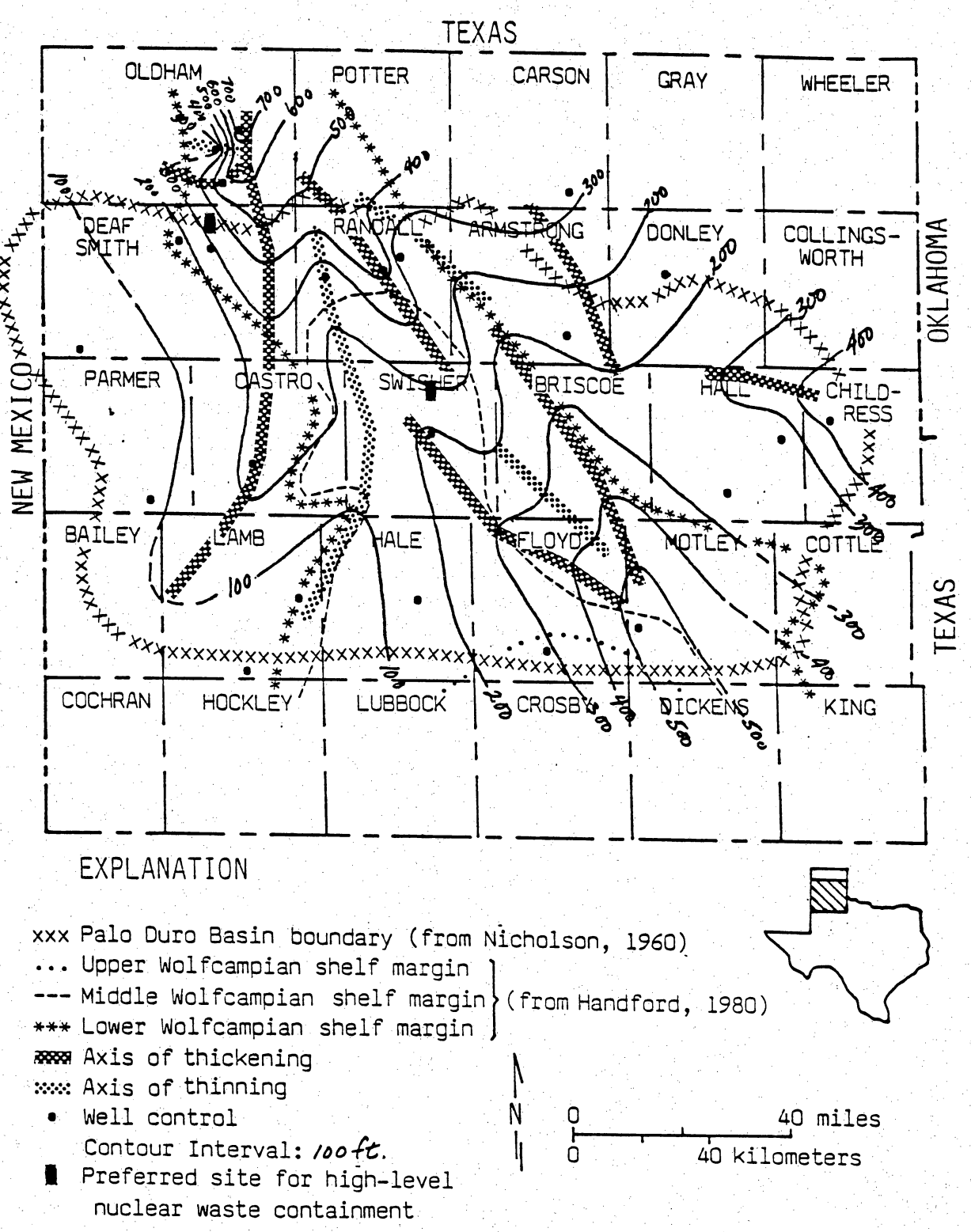

Figure 11. Net thickness of the >10-15% porosity range for the Wolfcamp.

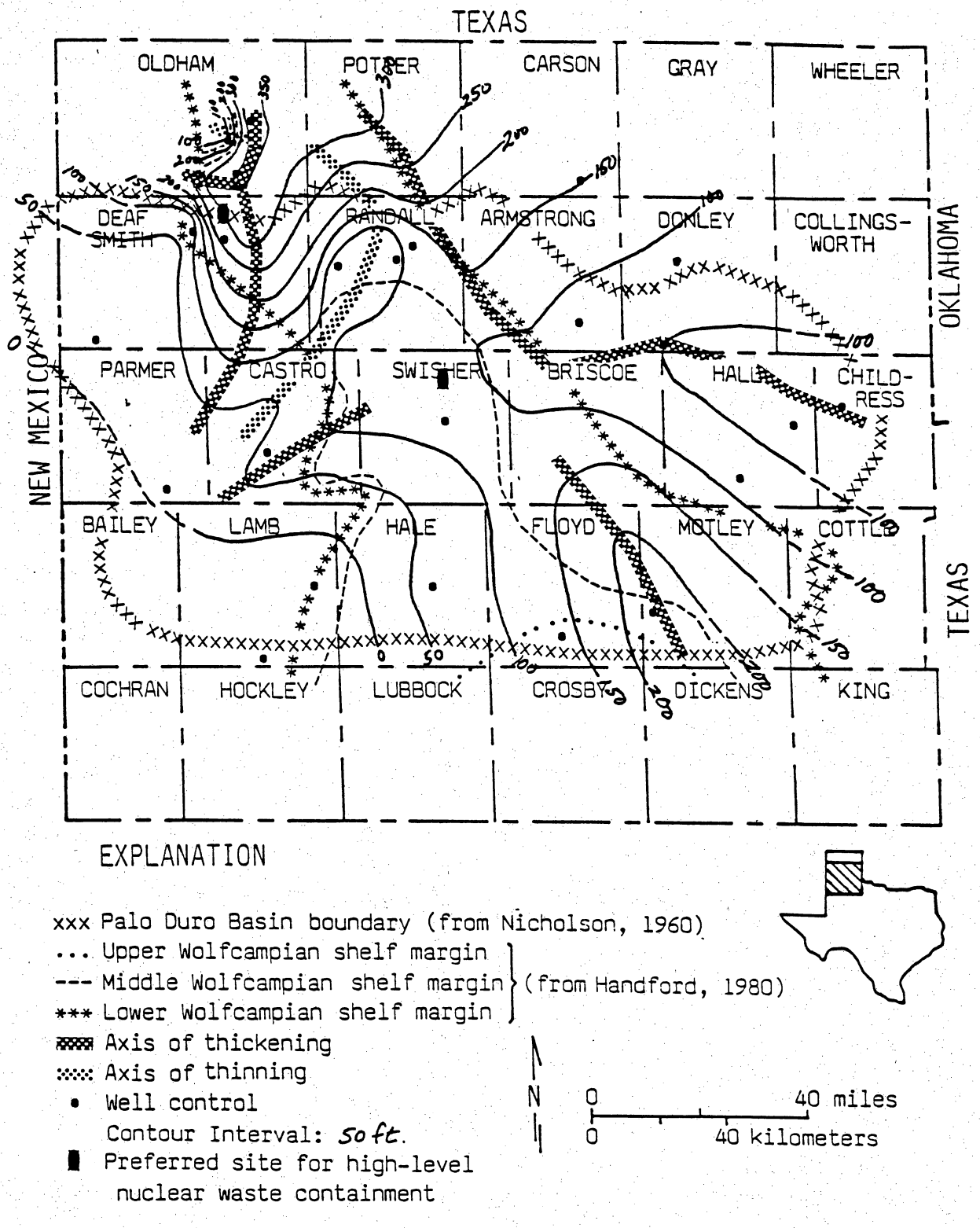

Figure 12. Net thickness of the >15-20% porosity range for the Wolfcamp.

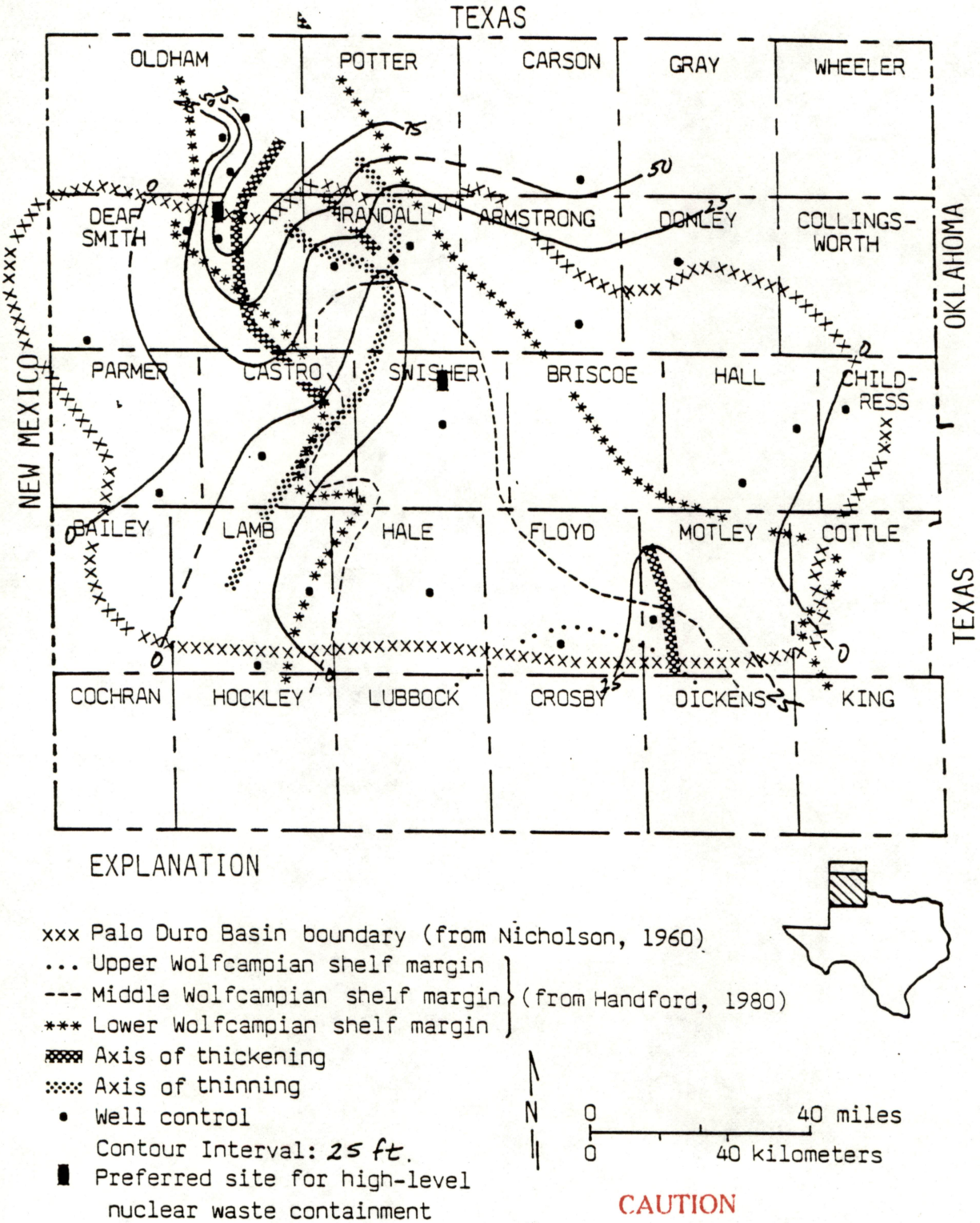

CAUTION

Figure 13. Net thickness of the >20-25% porosity range for the Wolfcamp.

This report describes research carried out by staff members of the Bureau of Economic Geology that addresses the feasibility of the Palo Duro Basin for isolation of high-level radioactive wastes. The report describes the progress and current status of research and tentative conclusions reached. Interpretations and conclusions are based on available data and state-of-the-art concepts, and hence, may be modified by more information and further application of the involved sciences.

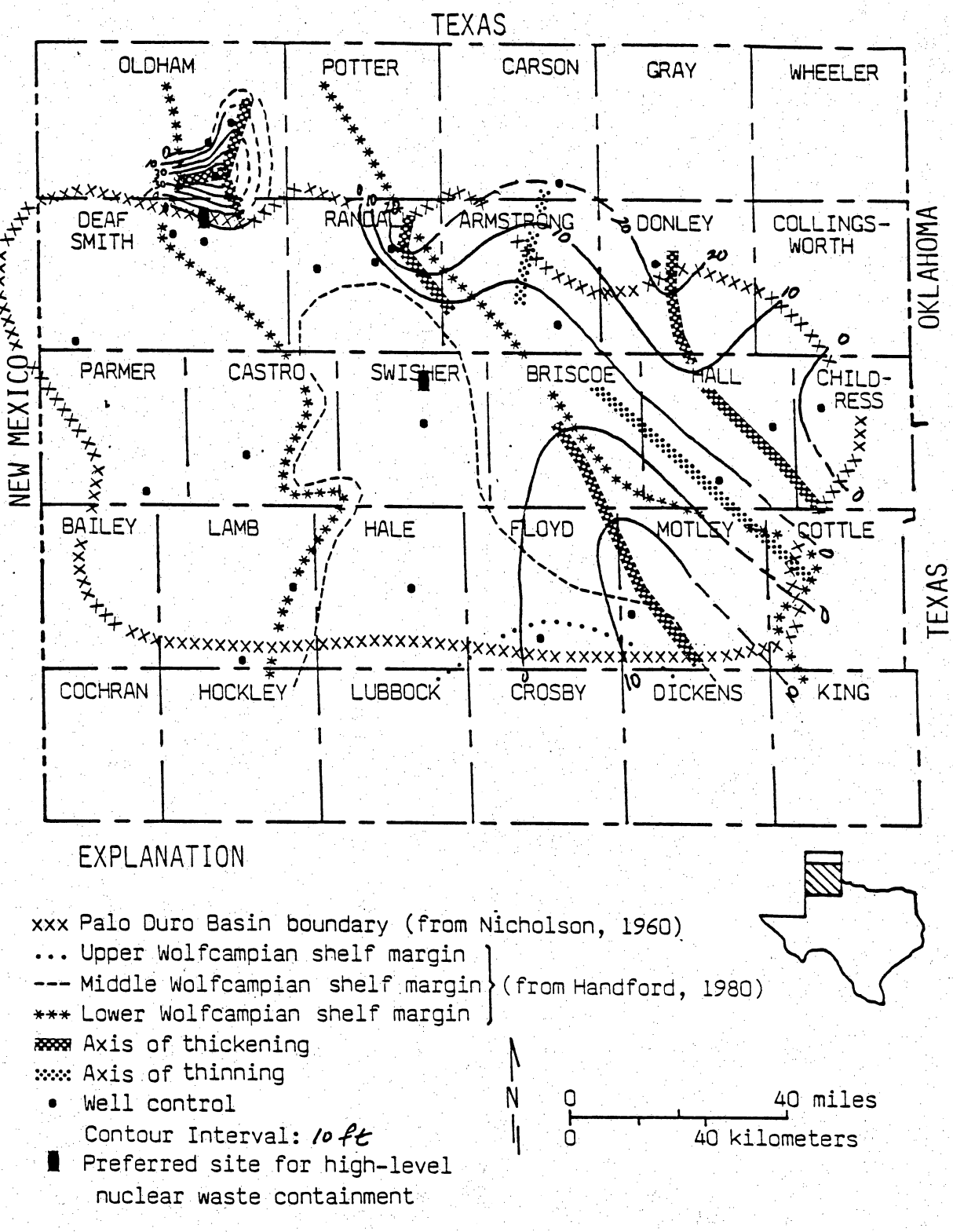

Figure 14. Net thickness of the >25-30% porosity range for the Wolfcamp.

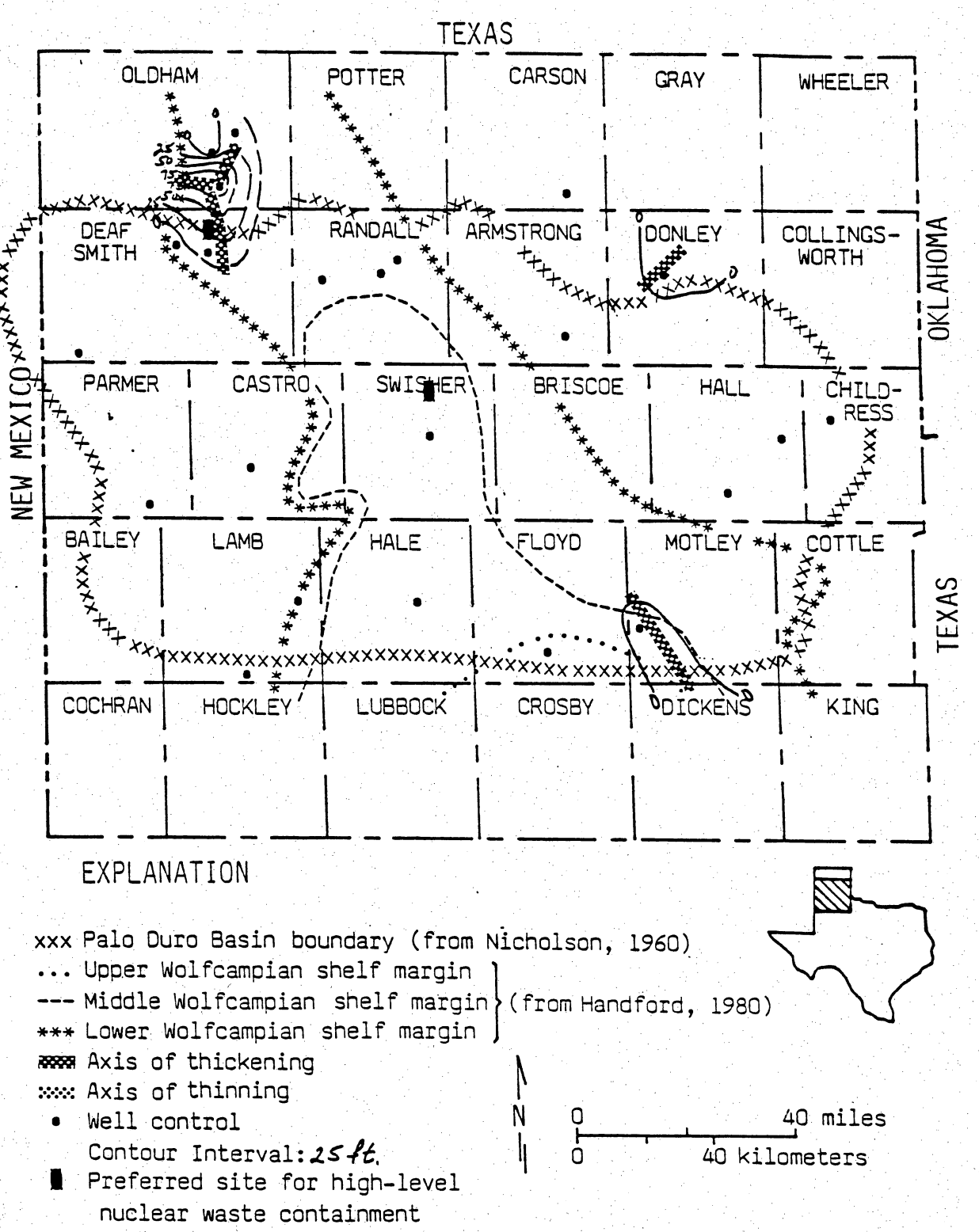

Figure 15. Net thickness of >30% porosity range for the Wolfcamp.

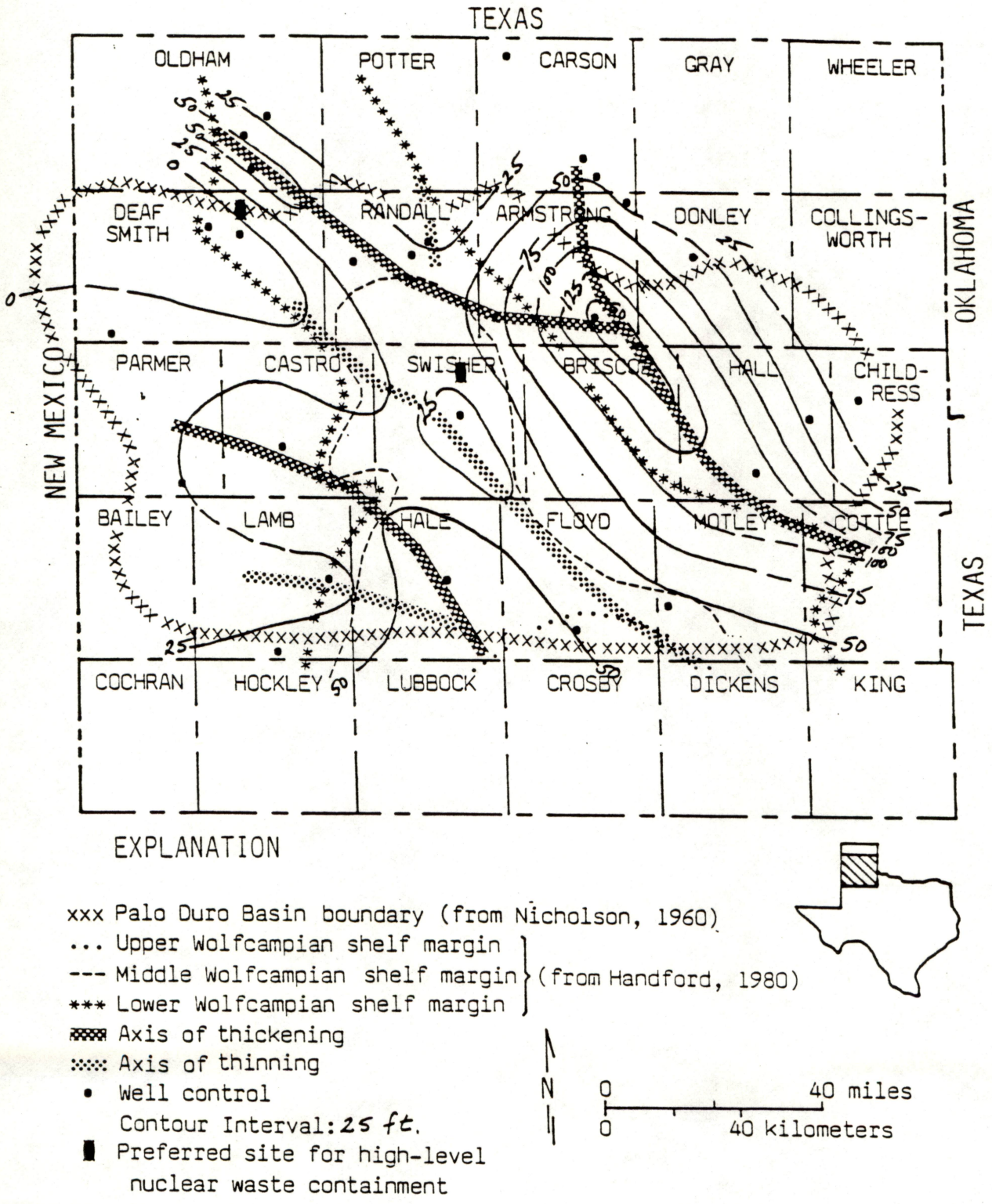

Figure 16. Net thickness of the 0-5% porosity range for the Brown Dolomite.

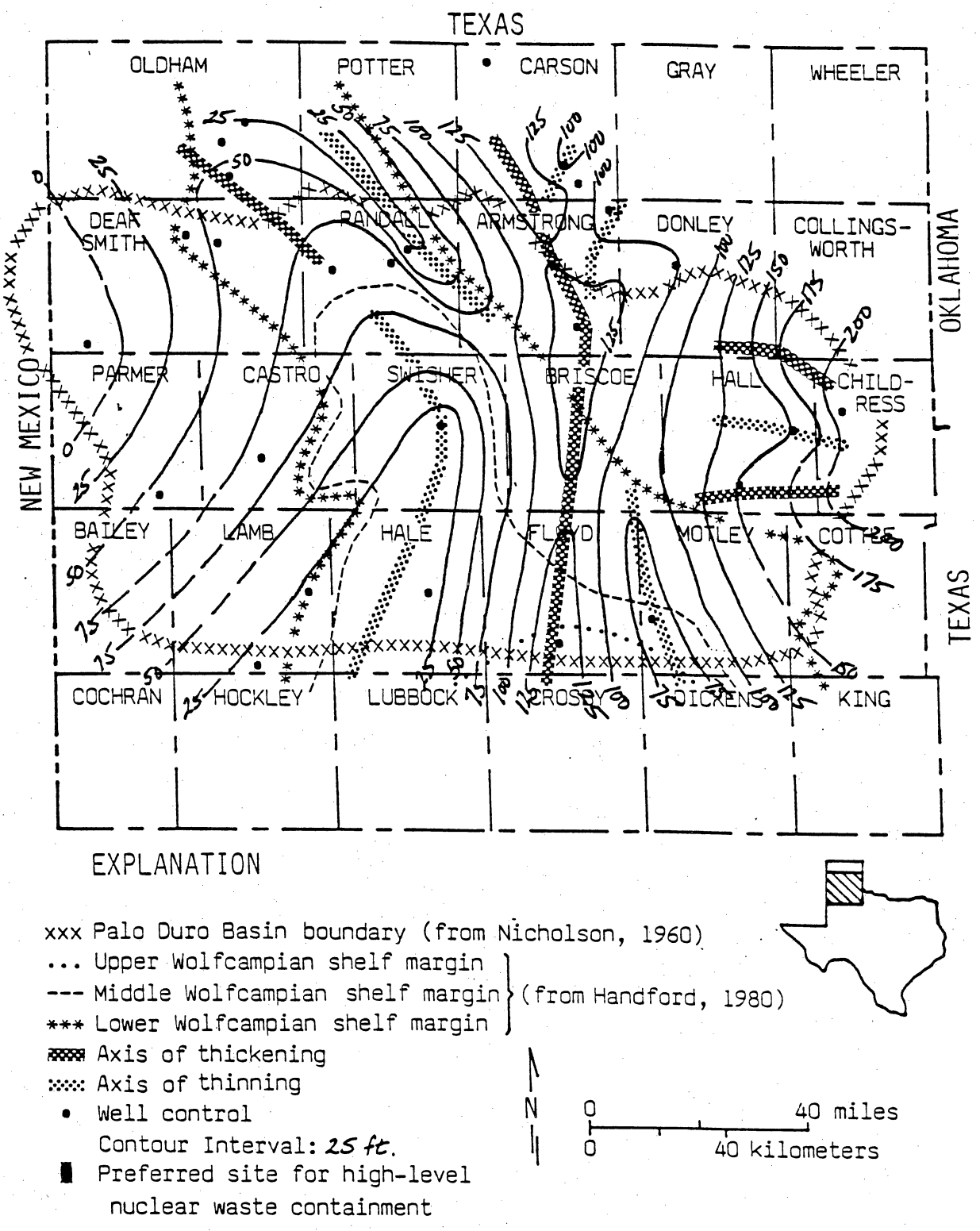

Figure 17. Net thickness of the >5-10% porosity range for the Brown Dolomite.

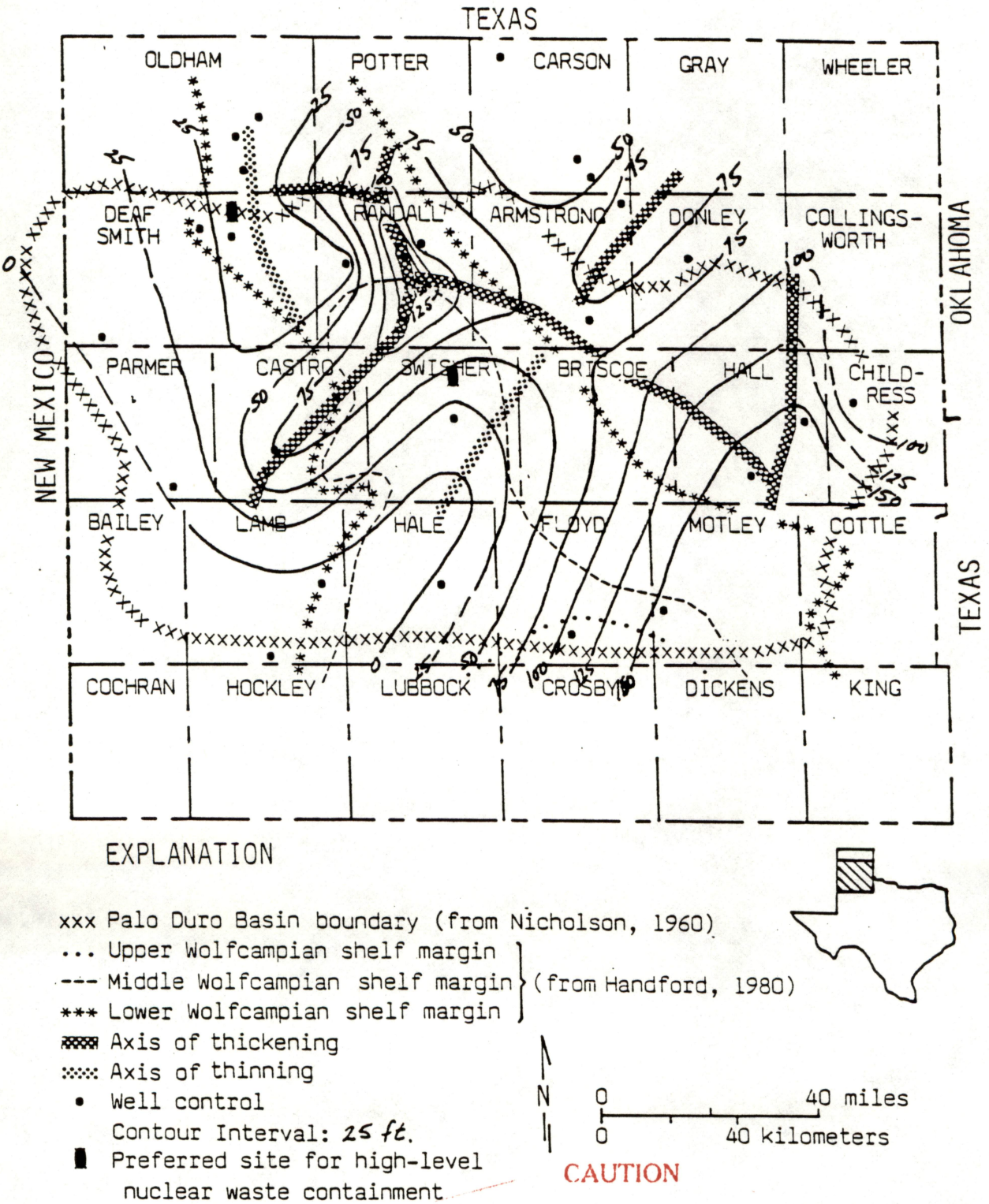

Figure 18. Net thickness of the >10-15% porosity range for the Brown Dolomite.

This report describes research carried out by staff members of the Bureau of Economic Geology that addresses the feasibility of the Palo Duro Basin for isolation of high-level nuclear wastes. The report describes the progress and current status of research and tentative conclusions reached. Interpretations and conclusions are based on available data and state-of-the-art concepts, and hence, may be modified by more information and further application of the involved sciences.

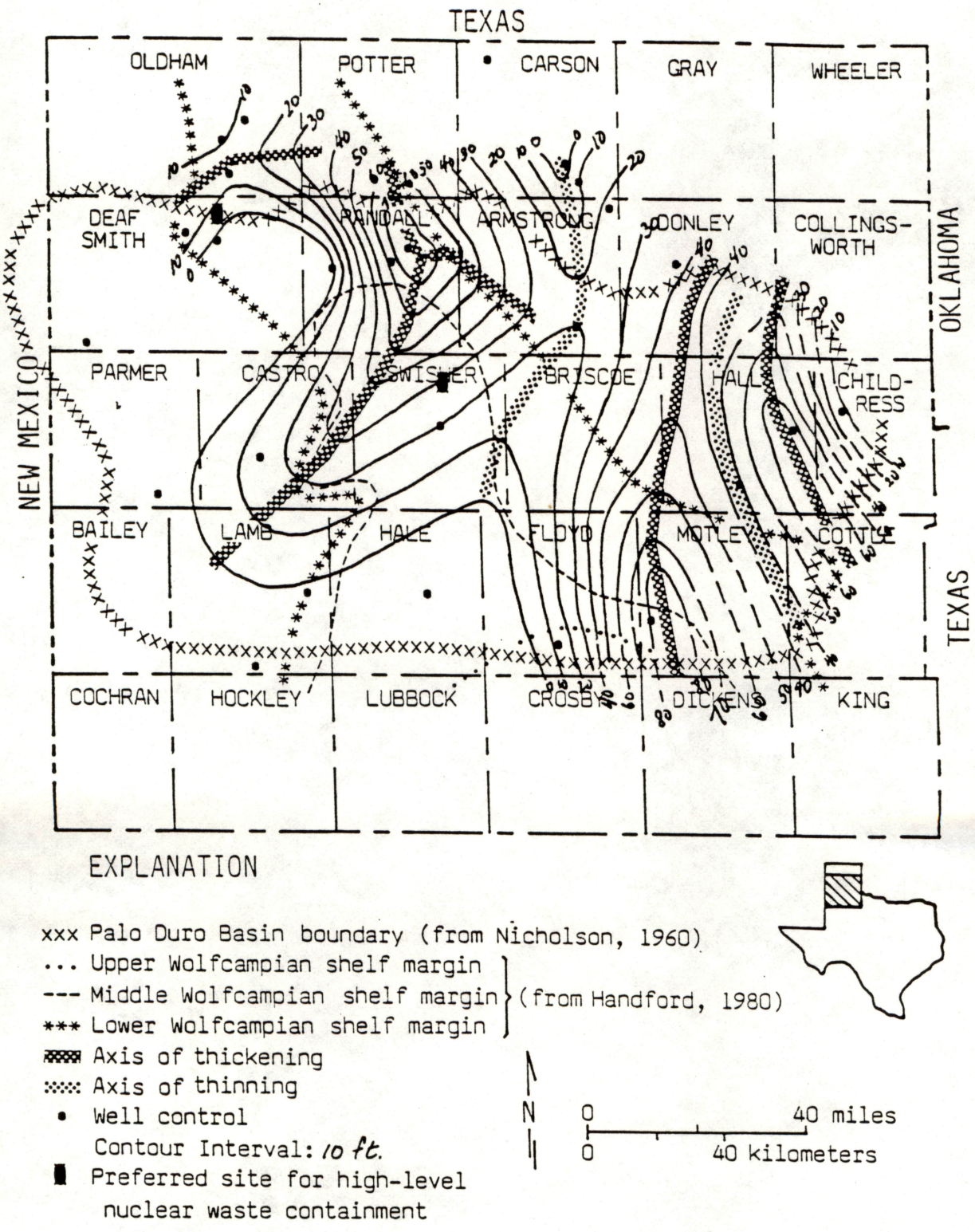

Figure 19. Net thickness of the >15-20% porosity range for the Brown Dolomite.

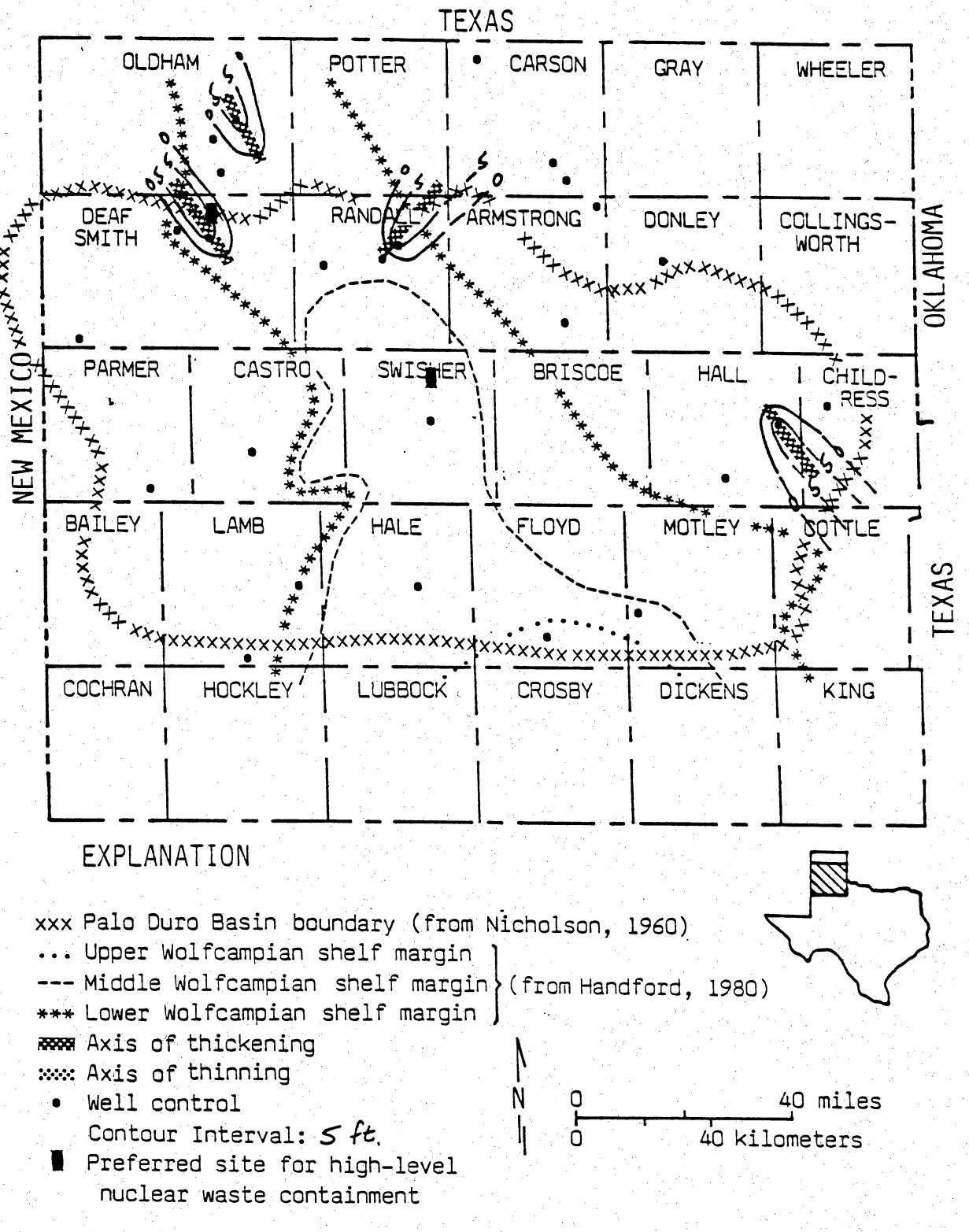

Figure 20. Net thickness of the >20-25% porosity range for the Brown Dolomite.

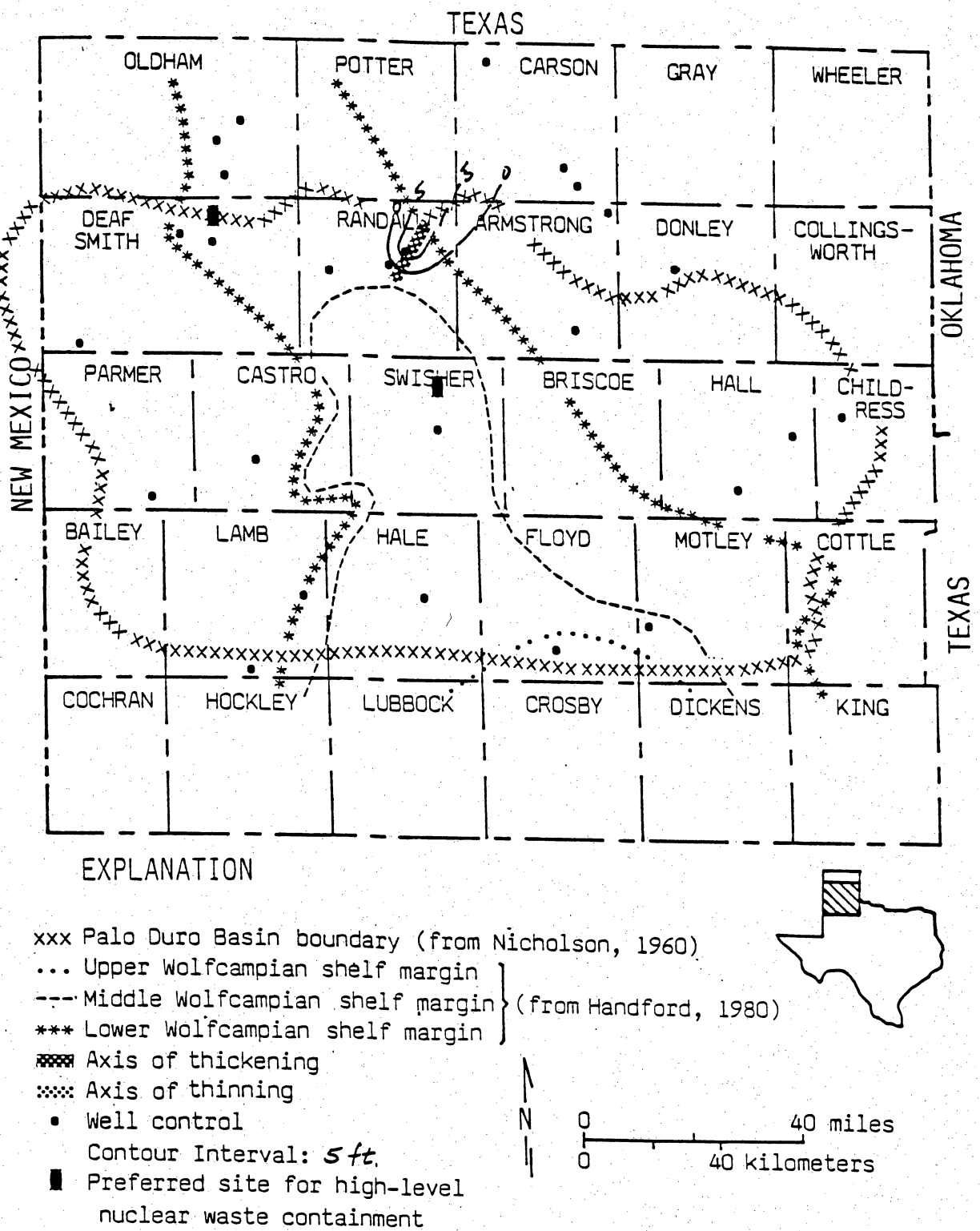

Figure 21. Net thickness of the >25-30% porosity range for the Brown Dolomite.

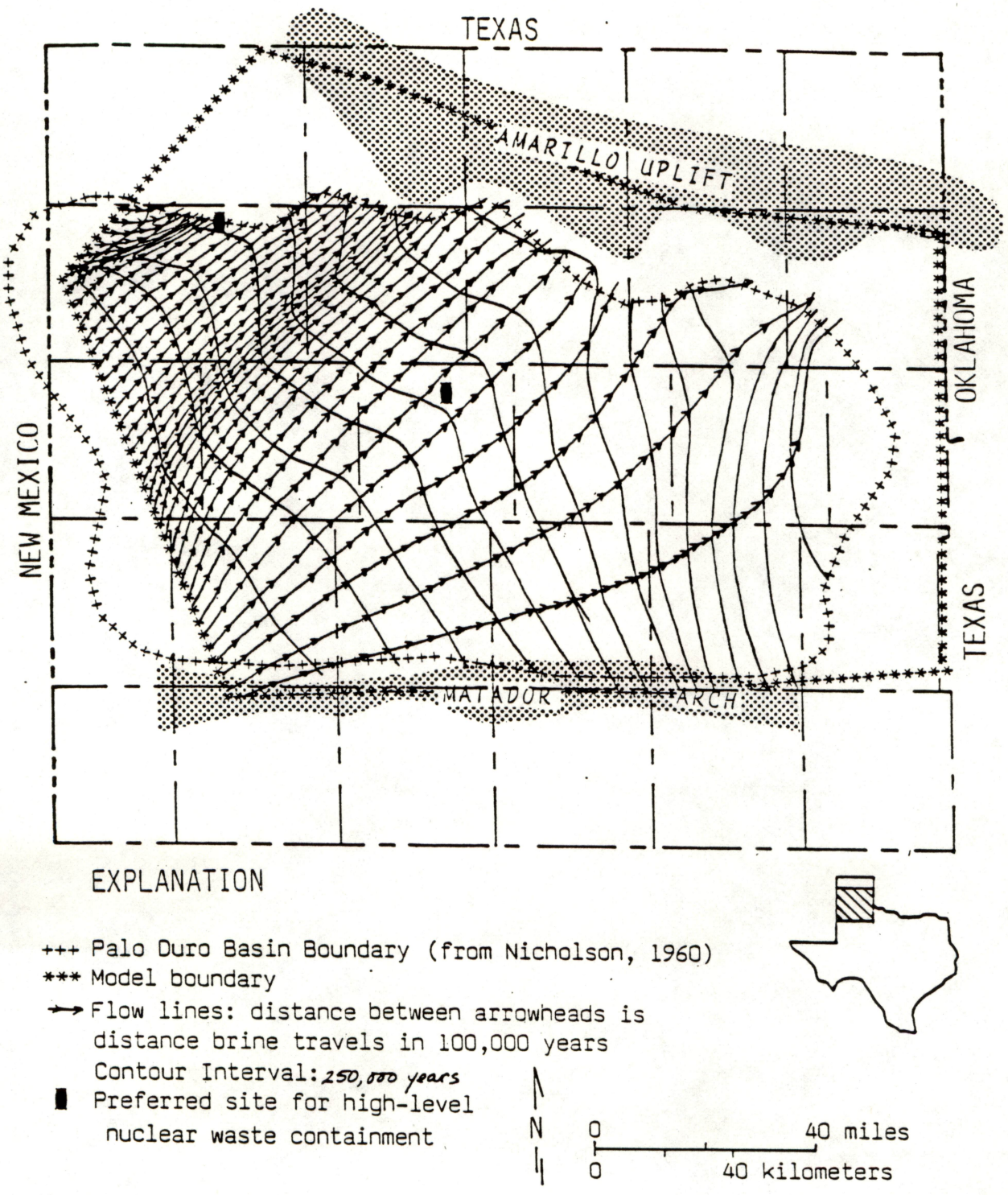

Figure 22. Areal model of northeastward ground-water flow in the Wolfcamp deep-basin aquifer, using typical porosity values, as described in the text.

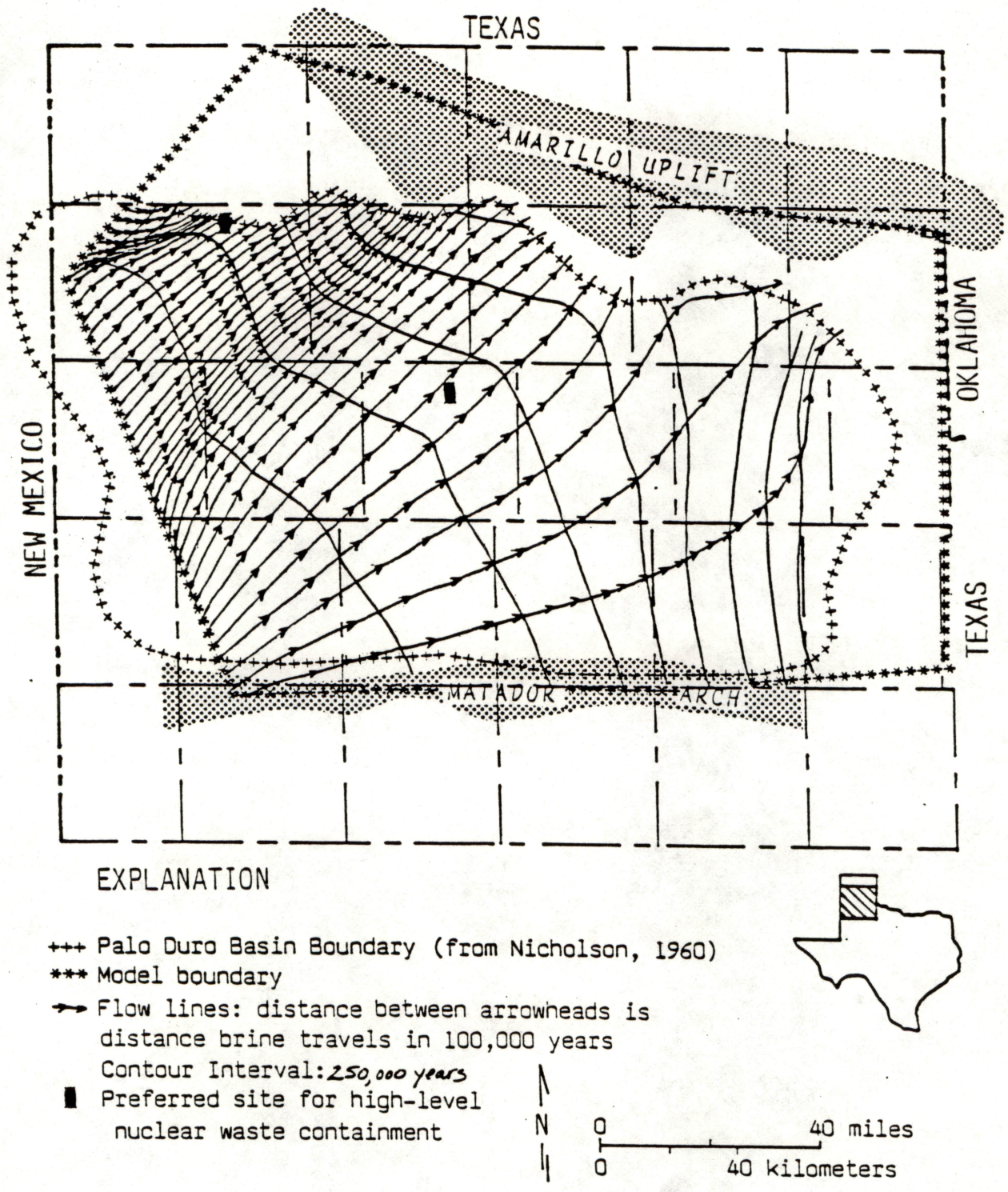

Figure 23. Areal model of northeastward ground-water flow in the Wolfcamp deep-basin aquifer, using average-porosity values derived from plotted and contoured porosity-log analyses, as described in the text and shown in figure 7.

TABLE 1.
List of Wells for which Neutron-Density Logs were run
to Obtain Wolfcamp Lithology and Porosity Determinations

N	County	BEG Well No.	Operator	Well Name	Approximate WOLFCAMP Depths (ft) Density porosity Neutron porosity X-Plot porosity X-Plot lithology
1	Armstrong	24	Paragon Resources, Inc.	J. A. Cattle Co. #1	3980-5170
2	Armstrong	42	Bryan Exploration Co.	Eschle #1-86	3350-4000 (T.D.)
3	Carson	2	Mesa Petroleum	Burnett #1-101	2550-3350 (T.D.)
4	Carson	38	Shenandoah Oil Corp.	Kotara #1	3050-3900 (T.D.)
5	Carson	39	Paradox Petroleum Co.	Friemel #1	3480-4580
6	Castro	21	Challenger Minerals, Inc.	J. R. Matthews #1	6190-7580
7	Childress	16	Corps of Engineers, Tulsa District	Jonah Creek #1	2610-3775
8	Deaf Smith	17	Voyager Petroleum Inc.	V. P. I. Reinauer #10-20	6430-7750
9	Deaf Smith	18	Buttes Resources Co.	Brorman #1	5700-7010
10	Deaf Smith	22	Stone & Webster Eng. Corp.	J. Friemel #1	5600-7120
11	Donley	32	Geochemical Surveys, Inc.	Harrison #1	3370-4160
12	Donley	50	Stone & Webster Eng. Corp.	Sawyer #1	2900-4015
13	Floyd	43	Argonot Energy Co.	Collins #1	4775-6695
14	Hale	57	Danigan Operating Co.	Tooker #1	5900-8050
15	Hall	30	R. D. Gunn	E. M. Timmons #1	3100-4365
16	Hall	33	Louisiana Land & Exploration Co.	O. C. Payne #1	2780-4220
17	Lamb	151	Gulf Energy & Minerals Co.-U.S.	James Blackwell et al. #1	7200-8550
18	Lamb	153	The Pickens Co., Inc.	J. W. Johnson #1	6500-7975
19	Motley	80	Koch Exploration Co.	H. H. Campbell #1	4900-7550
20	Oldham	77	Alpar Resources, Inc.	Middle Creek #1-35	4265-5435
21	Oldham	80	Page Petroleum	Scott 1-11	5150-6950
22	Oldham	84	Stone & Webster Eng. Corp.	Mansfield #1	4335-6610
23	Parmer	12	Convest Energy Corp.	O. L. Jarman #1	6550-7900
24	Randall	8	Pan Eastern Exploration Co.	Powers #1	4865-6375
25	Randall	13	Arkla Exploration Co.	Skypala #1-55	5100-6815
26	Randall	15	Arkla Exploration Co.	Kuhlman #1-83	4700-6560
27	Swisher	16	Stone & Webster Eng. Corp.	Zeeck #1	5368-7200

Table 2. Summary. Net Thicknesses of Seven Porosity Ranges in Wolfcamp Strata.

WELL County	BEG #	STRATIGRAPHIC UNIT (Net Thickness)	Porosity Range 0-5	>5-10	>10-15	>15-20	>20-25	>25-30	>30	ØAve
Armstrong	24	Brown Dolomite (383)	152	145	68	20	0	0	0	7.0
Armstrong	24	Wc < Brown Dolomite (783)	446	166	112	45	12	0	0	6.1
Armstrong	24	TOTAL (1166)	598	311	180	65	12	0	0	6.4
Armstrong	42	Brown Dolomite (243)	53	78	82	27	3	0	0	9.4
Armstrong	42	Wc < Brown Dolomite	ND	ND	ND	ND	ND	ND	ND	ND
Carson	2	Brown Dolomite (278)	240	194	34	10	0	0	0	9.6
Carson	2	Wc < Brown Dolomite	ND	ND	ND	ND	ND	ND	ND	ND
Carson	38	Brown Dolomite (207)	65	100	42	0	0	0	0	6.9
Carson	38	Wc < Brown Dolomite	ND	ND	ND	ND	ND	ND	ND	ND
Carson	39	Brown Dolomite (231)	51	130	40	10	0	0	0	7.7
Carson	39	Wc < Brown Dolomite (859)	137	190	296	147	68	21	0	11.8
Carson	39	TOTAL (1090)	188	320	336	157	68	21	0	10.9
Castro	21	Brown Dolomite (220)	38	90	75	17	0	0	0	9.1
Castro	21	Wc < Brown Dolomite (1169)	625	339	152	53	0	0	0	5.9
Castro	21	TOTAL (1389)	663	429	227	70	0	0	0	6.4

Table 2-continued

WELL County		STRATIGRAPHIC UNIT (Net Thickness)	Porosity Range 0-5	>5-10	>10-15	>15-20	>20-25	>25-30	>30	ØAve
Childress	16	Brown Dolomite (320)	11	214	85	10	0	0	0	9.0
Childress	16	Wc < Brown Dolomite (823)	420	217	86	100	0	0	0	6.7
Childress	16	TOTAL (1143)	431	431	171	110	0	0	0	7.3
Deaf Smith	17	Brown Dolomite (20)	10	0	10	0	0	0	0	7.5
Deaf Smith	17	Wc < Brown Dolomite (1248)	1060	132	37	19	0	0	0	3.6
Deaf Smith	17	TOTAL (1268)	1070	132	47	19	0	0	0	3.6
Deaf Smith	18	Brown Dolomite (90)	0	45	30	15	0	0	0	10.8
Deaf Smith	18	Wc < Brown Dolomite (1150)	568	365	162	50	5	0	0	6.2
Deaf Smith	18	TOTAL (1240)	568	410	192	65	5	0	0	6.6
Deaf Smith	24	Brown Dolomite (80)	0	55	20	0	5	0	0	9.7
Deaf Smith	24	Wc < Brown Dolomite (1367)	336	404	277	264	72	0	14	10.3
Deaf Smith	24	TOTAL (1447)	336	459	297	264	77	0	14	10.2
Donley	32	Brown Dolomite	ND	ND	ND	ND	ND	ND	ND	ND
Donley	32	Wc < Brown Dolomite (715)	480	145	75	15	0	0	0	4.9

Table 2-continued

WELL COUNTY	BEG #	STRATIGRAPHIC UNIT (Net thickness)	Porosity Range 0-5	>5-10	>10-15	>15-20	>20-25	>25-30	>30	ØAve
Donley	50	Brown Dolomite (277)	68	103	70	36	0	0	0	8.8
Donley	50	Wc < Brown Dolomite (779)	450	148	81	55	10	27	8	7.0
Donley	50	TOTAL (1056)	518	251	151	91	10	27	8	7.5
Floyd	43	Brown Dolomite (304)	50	136	108	10	0	0	0	8.8
Floyd	43	Wc < Brown Dolomite (1548)	1030	208	179	123	3	5	0	4.7
Floyd	43	TOTAL (1852)	1080	344	287	133	3	5	0	6.2
Hale	57	Brown Dolomite (73)	58	15	0	0	0	0	0	3.5
Hale	57	Wc < Brown Dolomite (1928)	1170	520	165	63	10	0	0	5.3
Hale	57	TOTAL (2001)	1228	535	165	63	10	0	0	5.2
Hall	30	Brown Dolomite (459)	110	150	159	40	0	0	0	8.9
Hall	30	Wc < Brown Dolomite (794)	446	214	114	15	5	0	0	5.7
Hall	30	TOTAL (1253)	556	360	273	55	5	0	0	6.8
Hall	33	Brown Dolomite (422)	45	150	157	65	5	0	0	10.5
Hall	33	Wc < Brown Dolomite (894)	460	281	90	58	0	5	0	6.0
Hall	33	TOTAL (1316)	505	431	247	123	5	5	0	7.6

Table 2-continued

WELL County	BEG #	STRATIGRAPHIC UNIT (Net Thickness)	Porosity Range 0-5	>5-10	>10-15	>15-20	>20-25	>25-30	>30	ØAve
Lamb	151	Brown Dolomite (48)	33	15	0	0	0	0	0	4.1
Lamb	151	Wc < Brown Dolomite (1227)	982	200	45	0	0	0	0	3.7
Lamb	151	TOTAL (1275)	1015	215	45	0	0	0	0	3.7
Lamb	153	Brown Dolomite (40)	20	20	0	0	0	0	0	5.0
Lamb	153	Wc < Brown Dolomite (1370)	917	389	59	0	5	0	0	4.3
Lamb	153	TOTAL (1410)	937	409	59	0	5	0	0	4.4
Motley	80	Brown Dolomite (372)	40	87	165	80	0	0	0	11.3
Motley	80	Wc < Brown Dolomite (1900)	756	575	346	150	40	18	15	7.9
Motley	80	TOTAL (2272)	796	662	511	230	40	18	15	8.5
Oldham	77	Brown Dolomite (93)	33	37	15	8	0	0	0	7.4
Oldham	77	Wc < Brown Dolomite (1032)	292	478	209	48	5	0	0	7.6
Oldham	77	TOTAL (1125)	325	515	224	56	5	0	0	7.6
Oldham	80	Brown Dolomite (147)	65	52	16	14	0	0	0	6.8
Oldham	80	Wc < Brown Dolomite (1601)	153	374	541	335	68	47	83	13.3
Oldham	80	TOTAL (1748)	218	426	557	349	68	47	83	12.8

Table 2-continued

WELL County	BEG #	STRATIGRAPHIC UNIT (Net Thickness)	Porosity Range 0-5	>5-10	>10-15	>15-20	>20-25	>25-30	>30	ØAve
Oldham	84	Brown Dolomite (74)	22	25	8	12	7	0	0	9.6
Oldham	84	Wc < Brown Dolomite (1998)	319	443	745	382	88	17	4	11.4
Oldham	84	TOTAL (2072)	341	468	753	394	95	17	4	11.3
Parmer	12	Brown Dolomite (90)	25	60	5	0	0	0	0	6.4
Parmer	12	Wc < Brown Dolomite (1090)	852	161	61	11	5	0	0	4.0
Parmer	12	TOTAL (1180)	877	221	66	11	5	0	0	4.2
Randall	8	Brown Dolomite (224)	14	26	96	72	8	8	0	13.8
Randall	8	Wc < Brown Dolomite (1216)	682	349	143	30	0	12	0	5.7
Randall	8	TOTAL (1440)	696	375	239	102	8	20	0	7.0
Randall	13	Brown Dolomite (126)	31	87	8	0	0	0	0	6.6
Randall	13	Wc < Brown Dolomite (1386)	557	495	246	81	7	0	0	7.0
Randall	13	TOTAL (1512)	588	582	254	81	7	0	0	7.0
Randall	15	Brown Dolomite (333)	34	78	156	65	0	0	0	11.3
Randall	15	Wc < Brown Dolomite (1468)	499	680	270	17	2	0	0	6.9
Randall	15	TOTAL (1801)	533	758	426	82	2	0	0	7.7
Swisher	16	Brown Dolomite (58)	13	10	15	20	0	0	0	11.1
Swisher	16	Wc < Brown Dolomite (1720)	1085	335	186	102	12	0	0	5.6
Swisher	16	TOTAL (1778)	1098	345	201	122	12	0	0	5.8

Table 3. Summary of volumetric calculations for Wolfcamp strata, based on twenty-seven lithology-porosity columns constructed from neutron-density porosity data.

POROSITY RANGE	MEAN POROSITY	SEDIMENT VOLUME		PORE VOLUME	
		(ft^3)	(m^3)	(ft^3)	(m^3)
0.00–0.05	0.025	2.359×10^{14}	6.679×10^{12}	5.398×10^{12}	1.670×10^{11}
>0.05–0.10	0.075	1.187×10^{14}	3.361×10^{12}	8.903×10^{12}	2.521×10^{11}
>0.10–0.15	0.125	6.583×10^{13}	1.864×10^{12}	8.229×10^{12}	2.330×10^{11}
>0.15–0.20	0.175	2.835×10^{13}	8.027×10^{11}	4.961×10^{12}	1.405×10^{11}
>0.20–0.25	0.225	3.877×10^{12}	1.098×10^{11}	8.723×10^{11}	2.470×10^{10}
>0.25–0.30	0.275	8.161×10^{11}	2.311×10^{10}	2.244×10^{11}	6.353×10^{9}
>0.30	0.325	5.817×10^{10}	1.647×10^{9}	1.891×10^{10}	5.354×10^{8}
	Total	4.535×10^{14}	1.284×10^{13}	2.911×10^{13}	8.242×10^{11}